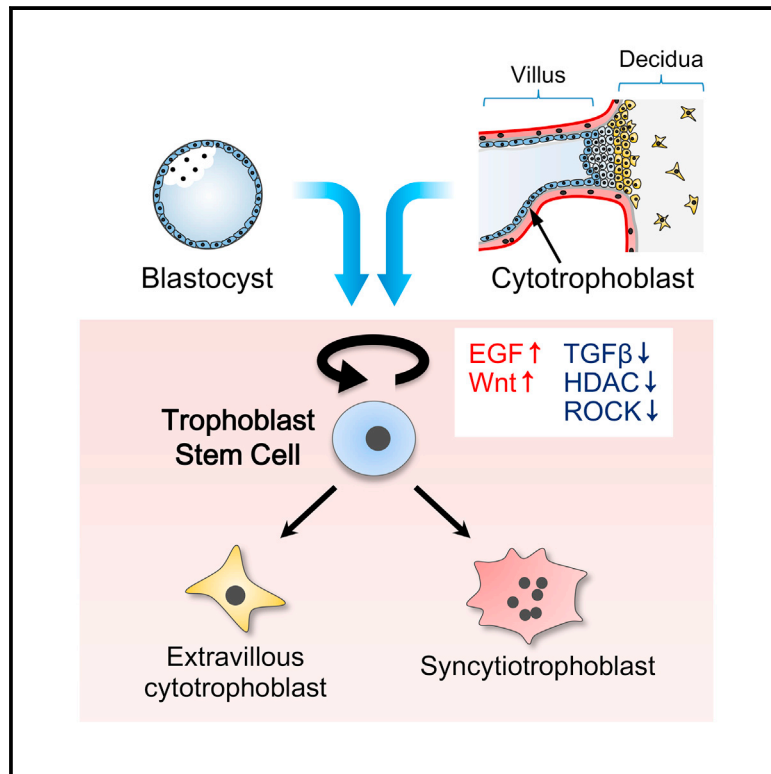


Cell Stem Cell

Derivation of Human Trophoblast Stem Cells

Graphical Abstract



Authors

Hiroaki Okae, Hidehiro Toh,
Tetsuya Sato, ..., Mikita Suyama,
Hiroyuki Sasaki, Takahiro Arima

Correspondence

okaehiro@m.tohoku.ac.jp (H.O.),
tarima@med.tohoku.ac.jp (T.A.)

In Brief

Trophoblast cells are specialized cells in the placenta that mediate the interactions between the fetus and mother. Okae et al. report the derivation of human trophoblast stem cells from blastocysts and early placentas, which will provide a powerful tool to study human placental development and function.

Highlights

- Human TS cells have the capacity to give rise to the three major trophoblast lineages
- Human TS and primary trophoblast cells have similar transcriptomes and methylomes
- Human TS cells injected into mice mimic trophoblast invasion during implantation
- Signaling pathways maintaining human and mouse TS cells are substantially different

Derivation of Human Trophoblast Stem Cells

Hiroaki Okae,^{1,6,*} Hidehiro Toh,² Tetsuya Sato,³ Hitoshi Hiura,¹ Sota Takahashi,¹ Kenjiro Shirane,^{2,4} Yuka Kabayama,^{2,5} Mikita Suyama,³ Hiroyuki Sasaki,² and Takahiro Arima^{1,*}

¹Department of Informative Genetics, Environment and Genome Research Center, Tohoku University Graduate School of Medicine, Sendai 980-8575, Japan

²Division of Epigenomics and Development, Medical Institute of Bioregulation, Kyushu University, Fukuoka 812-8582, Japan

³Division of Bioinformatics, Medical Institute of Bioregulation, Kyushu University, Fukuoka 812-8582, Japan

⁴Present address: Life Sciences Institute, Department of Medical Genetics, University of British Columbia, Vancouver, BC V6H 3N1, Canada

⁵Present address: MRC Centre for Regenerative Medicine, Institute for Stem Cell Research, School of Biological Sciences, University of Edinburgh, Edinburgh EH16 4UU, UK

⁶Lead Contact

*Correspondence: okaehiro@m.tohoku.ac.jp (H.O.), tarima@med.tohoku.ac.jp (T.A.)

<https://doi.org/10.1016/j.stem.2017.11.004>

SUMMARY

Trophoblast cells play an essential role in the interactions between the fetus and mother. Mouse trophoblast stem (TS) cells have been derived and used as the best *in vitro* model for molecular and functional analysis of mouse trophoblast lineages, but attempts to derive human TS cells have so far been unsuccessful. Here we show that activation of *Wingless/Integrated* (Wnt) and EGF and inhibition of TGF- β , histone deacetylase (HDAC), and Rho-associated protein kinase (ROCK) enable long-term culture of human villous cytotrophoblast (CT) cells. The resulting cell lines have the capacity to give rise to the three major trophoblast lineages, which show transcriptomes similar to those of the corresponding primary trophoblast cells. Importantly, equivalent cell lines can be derived from human blastocysts. Our data strongly suggest that the CT- and blastocyst-derived cell lines are human TS cells, which will provide a powerful tool to study human trophoblast development and function.

INTRODUCTION

The placenta is a multifunctional organ essential for fetal development and survival. Trophoblast cells are specialized cells in the placenta that mediate the interactions between the fetus and mother at the fetomaternal interface. In the human placenta, there are three major trophoblast subpopulations: the cytotrophoblast (CT), extravillous cytotrophoblast (EVT), and syncytiotrophoblast (ST) (Bischof and Irminger-Finger, 2005; James et al., 2012). CT cells are an undifferentiated and proliferative population that can give rise to EVT and ST cells. CT cells aggregate into cell columns at the tips of villi, where they differentiate into EVT cells. EVT cells can be subdivided based on their anatomical locations (Cierna et al., 2016). Those that invade the decidualized endometrium are called interstitial EVT cells. Those that invade and remodel the spiral arteries are

known as endovascular EVT. Other subtypes likely exist because EVT cells have also been found in uterine glands, veins, and lymphatics (Moser et al., 2010; Windsperger et al., 2017). Multinucleated ST cells are formed by fusion of CT cells and produce large quantities of placental hormones and other factors to maintain pregnancy. ST cells are directly in contact with maternal blood and mediate the exchange of gases and nutrients. All of the trophoblast lineages arise from the trophoblast (TE) cells of the blastocyst, and their coordinated proliferation and differentiation is essential for a successful pregnancy. Impaired trophoblast development and function are thought to lead to various pregnancy complications, including miscarriage, preeclampsia, and intrauterine growth restriction (Moffett and Loke, 2006; Norwitz, 2006).

Mouse trophoblast stem (TS) cells, which were first derived from blastocysts and the extra-embryonic ectoderm (ExE) of post-implantation embryos (Tanaka et al., 1998), are the best *in vitro* model for molecular and functional analysis of mouse trophoblast cells. In the presence of fibroblast growth factor 4 (FGF4) and transforming growth factor β 1 (TGF- β 1)/Activin, mouse TS cells self-renew indefinitely without losing their ability to differentiate into all trophoblast lineages. A number of transcription factors, including *Cdx2*, *Eomes*, *Elf5*, *Esrrb*, and *Gata3*, have been identified as essential for maintaining the undifferentiated state of mouse TS cells (Latos and Hemberger, 2016). Although it has been assumed that TE cells of human blastocysts and CT cells of early human placentas contain a stem cell population, attempts to derive human TS cells from these cells have so far been unsuccessful (Kunath et al., 2014; Soncin et al., 2015).

In this study, we analyzed the transcriptomes of primary trophoblast cells to infer how CT cells are maintained in their undifferentiated state *in vivo*. Using this knowledge, we optimized the culture conditions and derived human TS cells from CT cells and blastocysts. Our culture system will provide a powerful tool to study human trophoblast development and function.

RESULTS

Transcriptome Analysis of Primary Trophoblast Cells

We isolated CT, EVT, and ST cells from first-trimester placentas (Figures S1A–S1C) and performed RNA sequencing (RNA-seq)

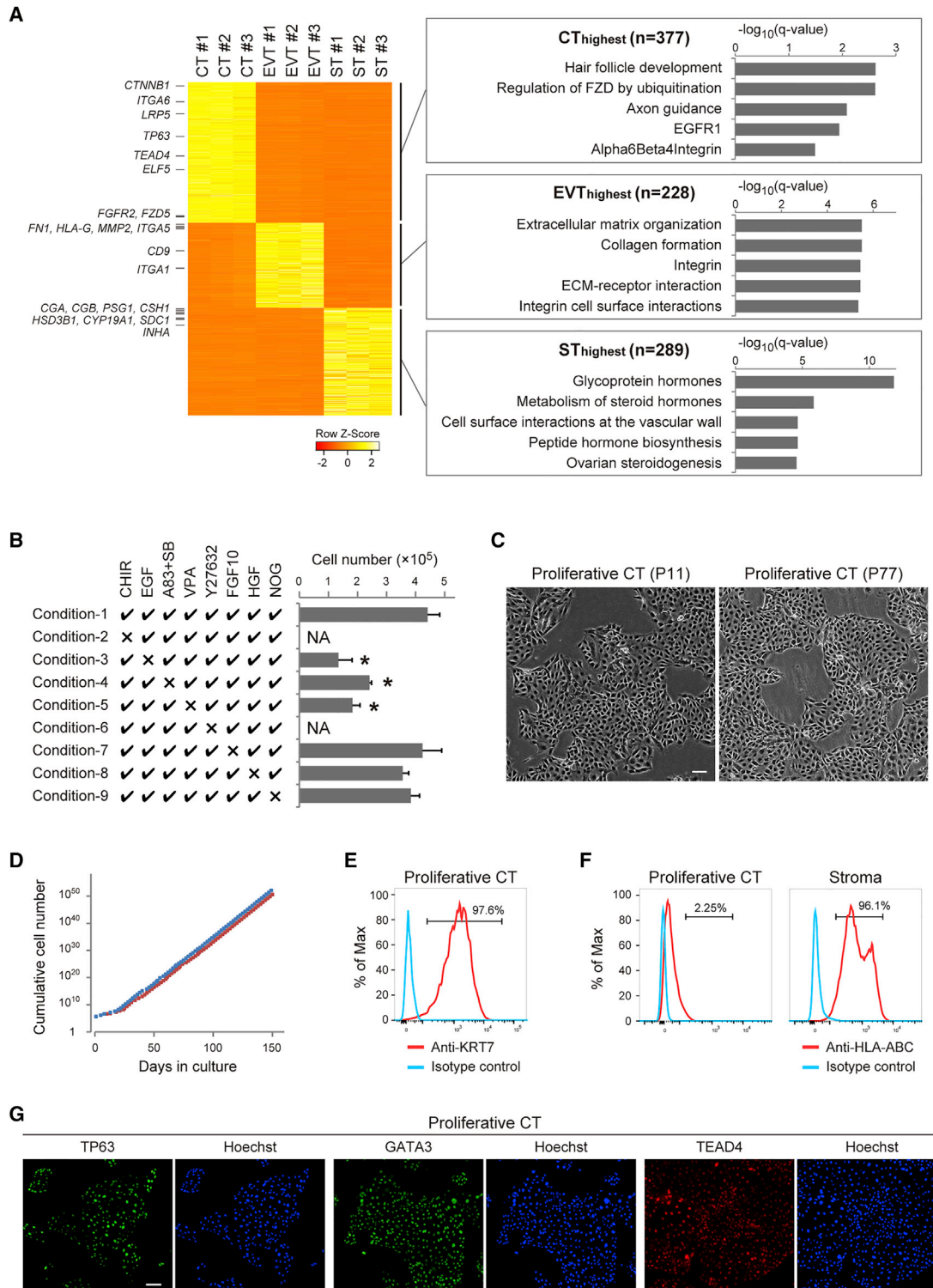


Figure 1. Transcriptome Profiling of Primary Trophoblast Cells and Establishment of Proliferative CT Cells in Culture

(A) Heatmap representation of Z score-transformed FPKM of genes predominantly expressed in CT, EVT, or ST cells (left). The RNA-seq data of CT cells are from our previous study (Hamada et al., 2016). The genes in each group are ranked in descending order according to their FPKM. Some representative lineage markers are indicated. Overrepresented pathways are shown on the right. The top five pathways are shown with q values.

(B) Screening of growth factors and inhibitors required for proliferation of CT cells *in vitro*. CT cells were cultured under the indicated conditions for 20 days. The cells were reseeded (1×10^5 cells per well in a 6-well plate) and counted after 2 days of culture. Data are presented as mean + SD (n = 3). Ticks and crosses

(legend continued on next page)

(Table S1). We identified 377, 228, and 289 genes that were predominantly expressed in CT, EVT, and ST cells, respectively (fragments per kilobase per million [FPKM] > 10 in the cell type with the highest expression, fold change > 4, adjusted $p < 0.01$) (Figure 1A). We confirmed that widely used lineage markers such as *ITGA6* and *TP63* (CT), *ITGA5* and *HLA-G* (EVT), and *CGB* and *CSH1* (ST) (Bischof and Irminger-Finger, 2005; Reis-Filho et al., 2003) were included in the gene lists. We then conducted functional annotation of the gene lists using ConsensusPathDB (Herwig et al., 2016; Figure 1A). Intriguingly, genes related to the Wntless/Integrated (Wnt) and epidermal growth factor (EGF) signal transduction pathways (“regulation of FZD by ubiquitination” and “EGFR1”) were overrepresented in the CT highest (CT_{highest}) gene list. Wnt and EGF signaling are required for proliferation of various epithelial stem cells, including skin stem cells and intestinal stem cells (Fatehullah et al., 2016; Hsu et al., 2014). Consistently, the top-ranked pathway for the CT_{highest} genes was “hair follicle development,” which included some genes important for the maintenance of hair follicle stem cells (*TP63*, *FGFR2*, and *CTNNB1* [encoding β -catenin]). These data imply that CT cells might be maintained under conditions similar to those of the other epithelial stem cells.

Establishment of Proliferative Human CT Cells in Culture

Based on the results described above, we tried to culture CT cells in a medium containing CHIR99021 (a Wnt activator) and EGF, but the cells did not adhere to the culture plate and died within several days. We then tested several inhibitors and growth factors (Figure 1B) that are known to enhance *in vitro* proliferation of various epithelial stem cells (Fatehullah et al., 2016). In the presence of all of these inhibitors and growth factors, highly proliferative cell lines were derived from CT cells (condition 1 in Figure 1B and Figure S1D). Among the inhibitors and growth factors, Y27632 (a Rho-associated protein kinase [ROCK] inhibitor) was found to be essential for cell attachment and was added to all culture media in subsequent experiments. CHIR99021 was indispensable for cell proliferation, and its absence led to differentiation of CT cells into HLA-G-positive EVT-like cells (Figure S1E). EGF, A83-01, and SB431542 (TGF- β inhibitors) and valproic acid (VPA) (a histone deacetylase [HDAC] inhibitor) significantly enhanced proliferation of CT cells (Figure 1B). Eventually, we found that CHIR99021, EGF, TGF- β inhibitors, VPA, and Y27632 together were sufficient for long-term culture of CT cells (Figure 1C). We were able to derive proliferative CT cells from as few as 1,000 CT cells (five cell lines from five independent experiments) but failed to derive TS cells from single CT cells ($n = 200$). CHIR99021, EGF, TGF- β inhibitors, and VPA

were all important for the long-term maintenance of proliferative CT cells (Figure S1F). VPA could be replaced by trichostatin A (TSA) or suberoylanilide hydroxamic acid (SAHA) (Figure S1G). Although either A83-01 or SB431542 could support the derivation of proliferative CT cells (Figure S1H), we retained both inhibitors in consideration of their different specificities (Vogt et al., 2011). The culture conditions tested in this study are summarized in Table S2.

We successfully derived proliferative CT cell lines from all first-trimester placental samples tested ($n = 8$) (Table S3). In contrast, we were unable to derive such cells from term placentas (placentas obtained after elective caesarean section, $n = 5$) under the same conditions. The proliferative CT cells had a normal karyotype (Figure S1I) and continued to proliferate for at least 5 months (~150 population doublings) (Figure 1D). These cells expressed a pan-trophoblast marker, KRT7 (Figure 1E), but HLA-ABC expression was very low (Figure 1F), which is a hallmark of CT cells (King et al., 2000). They also expressed TP63 and TEAD4 (CT markers) and GATA3 (a mononuclear trophoblast marker) (Figure 1G). The proliferative CT cells were designated CT-derived TS cells (TS^{CT} cells) because they had the ability to differentiate into EVT- and ST-like cells as detailed below.

Directed Differentiation of TS^{CT} Cells into EVT- and ST-like Cells

To analyze the differentiation potential of TS^{CT} cells, we first cultured TS cells in a basal medium containing only Y27632. Most of the cells differentiated into multinucleated ST-like cells, but some cells remained mononucleated (Figure S2A). The culture conditions did not support the survival of the differentiated cells, and most of them died within 5 days. Therefore, additional factor(s) may be required for the efficient and directed differentiation of TS^{CT} cells.

Matrigel is widely used to induce outgrowth of EVT cells from placental explants (Miller et al., 2005). A recent study also revealed that decidua-derived NRG1 promotes EVT formation in placental explant cultures (Fock et al., 2015). In addition, CT cells preferentially differentiated into EVT-like cells under condition 2 shown in Figure 1B (see also Figure S1E). Among the inhibitors and growth factors contained in condition 2, the TGF- β inhibitors were found to promote differentiation of CT cells into EVT-like cells, and A83-01 was more potent than SB431542 (Figure S2B). In a culture system containing NRG1, A83-01, and Matrigel (Figure 2A), TS^{CT} cells underwent epithelial-mesenchymal transition (Figure 2B; Figure S2C) and gave rise to EVT-like cells that strongly expressed HLA-G (Figure 2C). The resulting cells were named EVT-TS^{CT} cells. We confirmed that NRG1, A83-01, and Matrigel were all important for the induction of EVT-TS^{CT} cells (Figure S2D). *ITGA6* and *CDH1* (CT markers), *SDC1* (an ST

indicate included and excluded factors, respectively. Similar results were obtained with three independent placental samples. CHIR, CHIR99021; A83, A83-01; SB, SB431542; * $p < 0.01$ (Dunnett's test with condition 1 as a control); NA, not applicable.

(C) Phase-contrast images of proliferative CT cells at post-natal day 11 (P11) and P77.

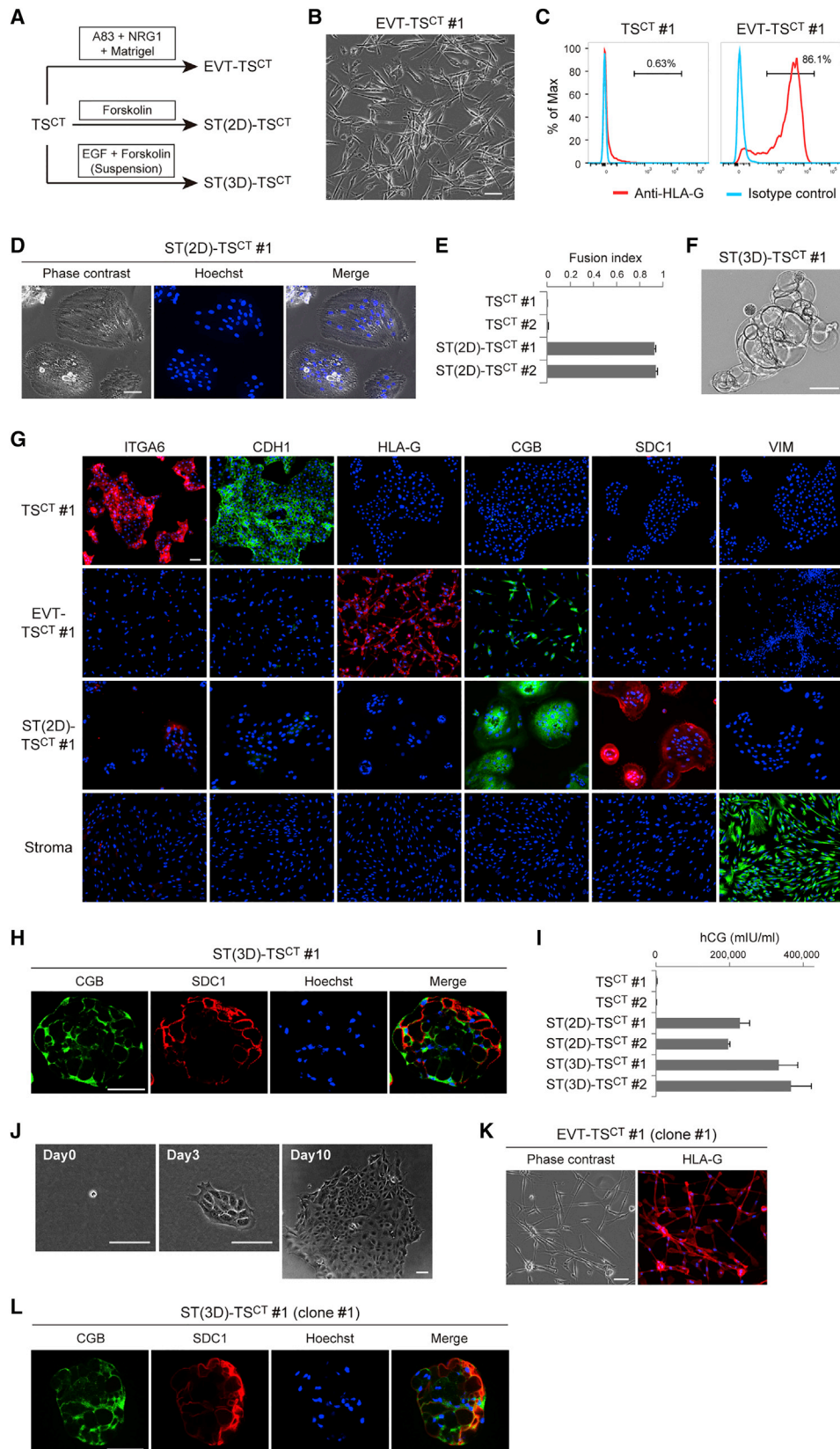
(D) Growth curve of proliferative CT cells. CT cells isolated from two placental samples were cultured for 5 months.

(E) Flow cytometry histogram of KRT7 expression in proliferative CT cells. Similar results were obtained with three independent cell lines.

(F) Flow cytometry histogram of HLA-ABC expression in proliferative CT cells. Similar results were obtained with three independent cell lines. Stromal cells derived from human placentas were analyzed as a positive control.

(G) Immunostaining of TP63, GATA3, and TEAD4 in proliferative CT cells. Nuclei were stained with Hoechst 33258. Similar results were obtained with three independent cell lines.

The scale bars indicate 100 μ m. See also Figure S1 and Tables S1, S2, and S3.



(legend on next page)

marker), and VIM (a stromal marker) expression was low or undetectable in EVT-TS^{CT} cells (Figure 2G). CGB (an ST marker) is expressed at low levels in EVT cells (Pröll et al., 2000) and, consistently, was detectable in EVT-TS^{CT} cells (Figure 2G).

Previous studies on choriocarcinoma cell lines revealed that cyclic AMP (cAMP) enhances ST formation (Strauss et al., 1992). Thus, we treated TS^{CT} cells with forskolin, a cAMP agonist (Figure 2A). In the presence of forskolin, the cells started to make aggregates and efficiently fused to form large syncytia (Figures 2D and 2E; Figure S2E). The ST markers CGB and SDC1 were highly expressed in these syncytia, whereas ITGA6, CDH1, HLA-G, and VIM were poorly expressed (Figure 2G). The ST-like syncytia were designated ST(2D)-TS^{CT} cells. It has also been reported that 3D culture enhances differentiation of choriocarcinoma cells into ST-like cells (McConkey et al., 2016). Therefore, we cultured the proliferative CT cells in low adhesion plates (Figure 2A). These cells formed cyst-like structures (Figure 2F), expressed CGB and SDC1 (Figure 2H), and secreted a large amount of human chorionic gonadotropin (hCG) (Figure 2I). Forskolin and EGF synergistically enhanced the formation of the cyst-like structures (Figure S2F). These cyst-like structures were designated ST(3D)-TS^{CT} cells. Expression of ST markers was higher in ST(3D)-TS^{CT} cells than in ST(2D)-TS^{CT} cells (Figure S2G).

TS^{CT} cells maintained their ability to differentiate into EVT- and ST-like cells after 50 passages (Figures S2H and S2I). We also cultured single TS^{CT} cells (n = 50) and isolated 10 clonal lines (Figure 2J). We randomly selected three clonal lines and confirmed that they could differentiate into both EVT- and ST-like cells (Figures 2K and 2L), suggesting that individual TS^{CT} cells were bipotent.

Establishment of Human TS Cells from Blastocysts

We next investigated whether cells similar to TS^{CT} cells could be derived directly from human blastocysts. Sixteen blastocysts were cultured under the same conditions (Figure 3A), and eight cell lines were established. These cell lines, designated blastocyst-derived TS cells (TS^{blast} cells), were morphologically similar to TS^{CT} cells (Figure 3B). A normal karyotype was confirmed in all six TS^{blast} cell lines examined (Figure S3A; Table S3). TS^{blast} cells continued to proliferate for at least 5 months (Figure 3B). As in the case of TS^{CT} cells, TS^{blast} cells expressed KRT7, TP63, GATA3,

and TEAD4 (Figures 3C and 3D), and HLA-ABC expression was very low (Figure S3B). Furthermore, TS^{blast} cells had the ability to differentiate into EVT-TS^{blast} (Figures 3E and 3F), ST(2D)-TS^{blast} (Figures 3G–3I), and ST(3D)-TS^{blast} cells (Figures 3J and 3K) just as TS^{CT} cells did (Figure 2A), although two TS^{blast} lines (4 and 7) differentiated into EVT-like cells less efficiently than the other TS^{blast} and TS^{CT} lines (Figures S3C and S3D). The differentiation ability of TS^{blast} cells was maintained after 55 passages (Figures S3E and S3F). We also cultured single TS^{blast} cells (n = 50) and isolated 8 clonal lines. We randomly selected three clonal lines and confirmed that they could differentiate into both EVT- and ST-like cells (Figures 3L and 3M).

Transcriptome Profiling of Human TS Cells

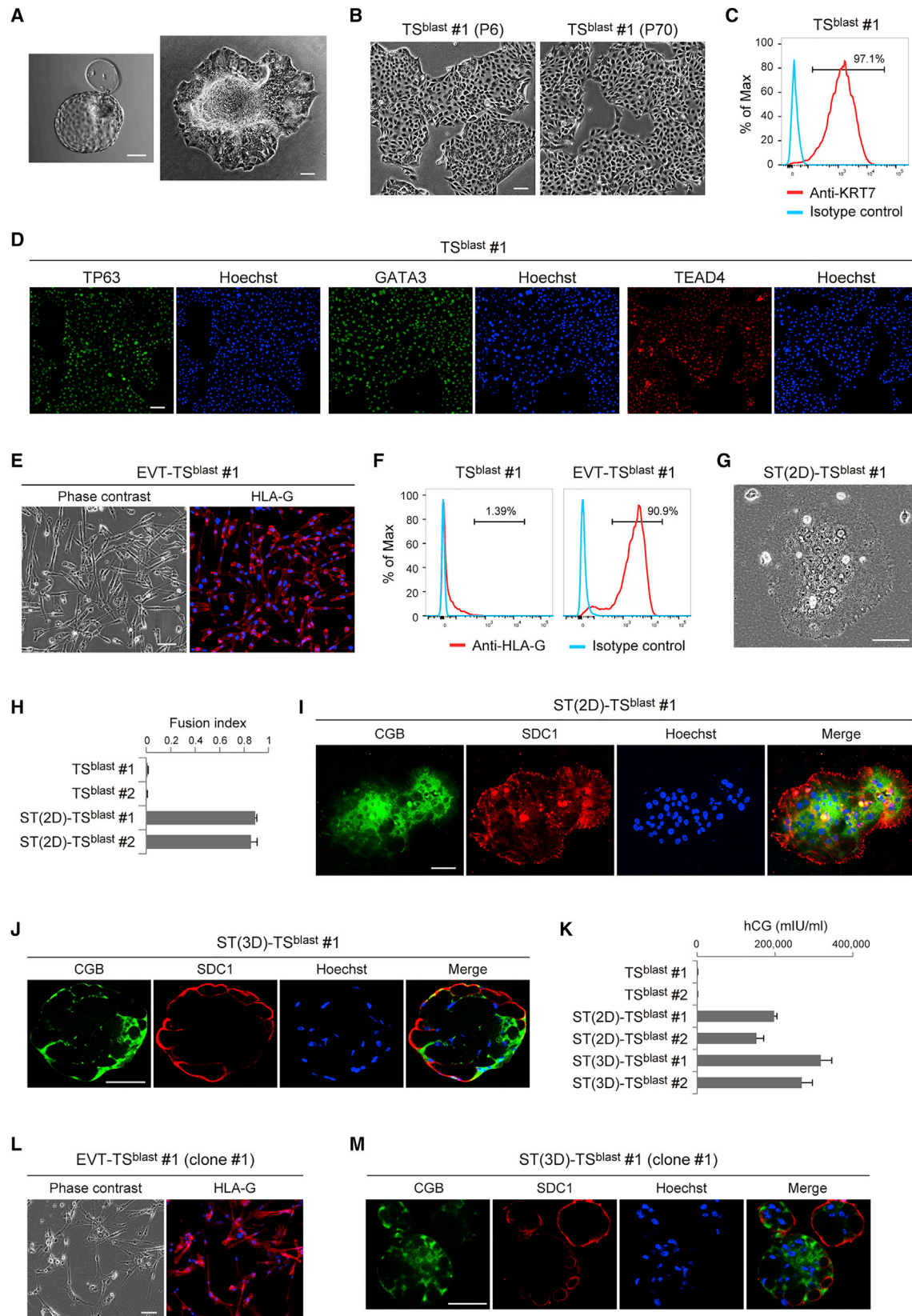
To determine whether TS^{CT} and TS^{blast} cells had gene expression patterns similar to primary trophoblast cells, we performed RNA-seq of TS^{CT} and TS^{blast} cells and their derivatives (Figure 4A). A preliminary investigation suggested that ST(2D) and ST(3D) cells had very similar transcriptome profiles, but ST(3D) cells were a little more similar to primary ST cells (Figure S4A). Therefore, we chose ST(3D) cells as the model of ST cells. We compared the RNA-seq data with those of primary trophoblast cells and placenta-derived stromal cells. Hierarchical clustering revealed that TS^{CT} and TS^{blast} cells had very similar gene expression patterns to each other, both before and after their differentiation ($R > 0.98$) (Figure 4A). Importantly, the gene expression profiles of CT cells were closest to those of TS^{CT} and TS^{blast} cells (Figure 4A). The profiles of TS^{CT}- and TS^{blast}-derived EVT- and ST-like cells were closely related to those of primary EVT and ST cells, respectively (Figure 4A). Furthermore, most of the genes predominantly expressed in CT, EVT, or ST cells (the genes shown in Figure 1A) showed similar expression patterns in TS^{CT} and TS^{blast} cells and their derivatives (Figure 4B). We then focused on some representative lineage markers. All CT markers we examined exhibited the expected expression patterns, although some genes, such as *LRP5*, *TP63*, and *ELF5*, showed lower expression in TS^{CT} and TS^{blast} cells (Figure 4C). Most EVT and ST markers also showed comparable expression patterns and levels in the primary and cultured cells, with a few exceptions (e.g., *CD9* and *CSH1*) (Figures 4D and 4E).

Although TS^{CT} and TS^{blast} cells had gene expression profiles similar to those of primary cells, they were not exactly the

Figure 2. Directed Differentiation of TS^{CT} Cells into EVT- and ST-like Cells

- (A) Schematic representation of protocols for directed differentiation of TS^{CT} cells.
 (B) Phase contrast image of EVT-TS^{CT} cells. EVT-TS^{CT} cells have a mesenchyme-like morphology.
 (C) Flow cytometry histograms of HLA-G expression on TS^{CT} and EVT-TS^{CT} cells. Similar results were obtained with three independent cell lines.
 (D) Phase-contrast and Hoechst staining images of ST(2D)-TS^{CT} cells.
 (E) Fusion efficiency of ST(2D)-TS^{CT} cells. The fusion index is defined as (N-S)/T, where N is the number of nuclei in the syncytia, S is the number of syncytia, and T is the total number of nuclei counted. Data are presented as mean + SD (n = 3).
 (F) Phase-contrast image of ST(3D)-TS^{CT} cells.
 (G) Immunostaining of ITGA6 and CDH1 (CT markers), HLA-G (an EVT marker), CGB and SDC1 (ST markers), and VIM (a stromal marker) in TS^{CT}, EVT-TS^{CT}, and ST(2D)-TS^{CT} cells. Similar results were obtained with two independent cell lines. Stromal cells derived from human placentas were analyzed for comparison.
 (H) Confocal images of ST(3D)-TS^{CT} cells stained for CGB and SDC1. Similar results were obtained with three independent cell lines.
 (I) Levels of hCG secreted by TS^{CT}, ST(2D)-TS^{CT}, and ST(3D)-TS^{CT} cells. Data are presented as mean + SD (n = 3).
 (J) Phase-contrast images showing the growth of a single TS^{CT} cell.
 (K) Phase-contrast and immunofluorescence images of EVT-like cells derived from a clonal TS^{CT} line. The cells were stained for HLA-G. Similar results were obtained with three clonal lines derived from TS^{CT} 1.
 (L) Confocal images of ST(3D) cells derived from a clonal TS^{CT} line. The cells were stained for CGB and SDC1. Similar results were obtained with three clonal lines derived from TS^{CT} 1.

The scale bars indicate 100 μ m. See also Figure S2.



(legend on next page)

same, presumably reflecting the artificial *in vitro* conditions. Gene set enrichment analysis (GSEA) revealed that genes associated with various gene ontology (GO) terms were differentially expressed between the primary and cultured cells. Notably, genes related to ribosome biogenesis were especially enriched in TS cells (Figure S4B), which might contribute to TS cell proliferation because ribosomes drive cell proliferation and growth. We also found that DNA replication-related genes were significantly depleted in TS-derived EVT-like cells (Figure S4C), consistent with our observation that TS cells differentiating into EVT-like cells gradually lost their proliferative capacity.

Several genes such as *CYP19A1*, *EDNRB*, *IL2RB*, and *PTN* are reported to have placenta-specific promoters (Cohen et al., 2011; Rawan and Cross, 2008). We found that these placenta-specific promoters were active in ST(3D)-TS^{CT} and ST(3D)-TS^{blast} cells (Figure S4D). As shown in Figure 4C, *FGFR2* was predominantly expressed in CT cells and undifferentiated TS^{CT} and TS^{blast} cells. We found that, of the two major isoforms of *FGFR2* (*FGFR2b* and *FGFR2c*), *FGFR2b* was expressed almost exclusively (Figure S4E). This is intriguing because the essential role of *Fgfr2c* was reported in mouse trophoblast cells (Arman et al., 1998). Furthermore, *CDX2*, *EOMES*, *ESRRB*, and *SOX2*, which encode transcription factors required for mouse TS cell self-renewal (Latos and Hemberger, 2016), were poorly expressed (< 1 FPKM) in CT, TS^{CT}, and TS^{blast} cells (Table S1).

DNA Methylome Profiling of Human TS Cells

Trophoblast cells have unique DNA methylation patterns characterized by large partially methylated domains (PMDs) (Schroeder et al., 2013), placenta-specific promoter hypomethylation (Robinson and Price, 2015), and placenta-specific germline differentially methylated regions (gDMRs) (Court et al., 2014). To examine whether these unique methylation patterns were maintained in TS^{CT} and TS^{blast} cells, we performed whole-genome bisulfite sequencing (WGBS) of TS^{CT} and TS^{blast} cells and compared the data with those of CT cells (Hamada et al., 2016), human embryonic stem cells (ESCs) (Lister et al., 2011),

and cord blood cells (Okae et al., 2014) (Figure 5A). TS^{CT} and TS^{blast} cells showed almost identical global DNA methylation patterns ($R = 0.97$). Although the average methylation levels of TS^{CT} (33.7%) and TS^{blast} cells (33.6%) were substantially lower than that of CT cells (52.3%), their methylation patterns were similar to each other ($R \geq 0.80$). Most of the PMDs defined in a previous study (Schroeder et al., 2013) maintained the intermediate methylation levels in CT cells but were hypomethylated in TS^{CT} and TS^{blast} cells (Figures 5B and 5C). Actively transcribed regions showed higher methylation levels compared with other regions in CT, TS^{CT}, and TS^{blast} cells (Figure S5A), consistent with previous findings in the human placenta (Schroeder et al., 2013). Therefore, the placenta-specific DNA methylome was largely maintained in TS^{CT} and TS^{blast} cells, although the cause and significance of the PMD hypomethylation remain unclear.

We next analyzed the *ELF5* promoter, which is hypomethylated in trophoblast cells but hypermethylated in many other cell types (Hemberger et al., 2010). We found that the *ELF5* promoter was hypomethylated in both TS^{CT} and TS^{blast} cells (Figure 5D). In addition to the *ELF5* promoter, we identified 55 promoters with methylation patterns similar to that of the *ELF5* promoter (methylation level < 20% in CT cells and > 80% in ESCs and blood cells), which included some promoters that are known to be specifically hypomethylated in the placenta (e.g., the promoters of *INSL4* and *DSCR4*) (Du et al., 2011; Macaulay et al., 2011). We found that most of these promoters (48 of 55) maintained less than 20% methylation levels in TS^{CT} and TS^{blast} cells (Figure 5E; Table S4). We confirmed the hypomethylation of three selected promoters (*DSCR4*, *ELF5*, and *ZNF750*) in all TS^{CT} and TS^{blast} lines established in this study (Figure S5B). We also identified 5 promoters with the opposite pattern, and all of them had more than 80% methylation levels in TS^{CT} and TS^{blast} cells (Figure 5E; Table S4).

A number of placenta-specific gDMRs, which maintain allele-specific DNA methylation in a placenta-specific manner, have been identified. We focused on placenta-specific gDMRs associated with imprinted genes ($n = 33$) (Table S5). Most of the gDMRs maintained the expected intermediate methylation levels

Figure 3. Derivation and Directed Differentiation of TS^{blast} Cells

- (A) Left: representative oblique illumination image of a hatched human blastocyst 7 days post-fertilization. Right: representative phase-contrast image of a blastocyst outgrowth 8 days post-fertilization.
- (B) Phase-contrast images of TS^{blast} cells at P6 and P70. TS^{blast} cells continued to proliferate for at least 5 months. Similar results were obtained with two independent cell lines.
- (C) Flow cytometry histogram of KRT7 expression in TS^{blast} cells. Similar results were obtained with three independent cell lines.
- (D) Immunostaining of TP63, GATA3, and TEAD4 in TS^{blast} cells. Nuclei were stained with Hoechst 33258. Similar results were obtained with three independent cell lines.
- (E) Phase-contrast and immunofluorescence images of EVT-TS^{blast} cells. The cells were stained for HLA-G. Similar results were obtained with three independent cell lines.
- (F) Flow cytometry histograms of HLA-G expression in TS^{blast} and EVT-TS^{CT} cells. Similar results were obtained with three independent cell lines.
- (G) Phase-contrast image of ST(2D)-TS^{blast} cells.
- (H) Fusion indices of TS^{blast} and ST(2D)-TS^{blast} cells.
- (I) Immunostaining of CGB and SDC1 in ST(2D)-TS^{blast} cells. Similar results were obtained with three independent cell lines.
- (J) Confocal images of ST(3D)-TS^{blast} cells stained for CGB and SDC1. Similar results were obtained with three independent cell lines.
- (K) Levels of hCG secreted by TS^{blast}, ST(2D)-TS^{blast}, and ST(3D)-TS^{blast} cells. Data are presented as mean + SD ($n = 3$).
- (L) Phase-contrast and immunofluorescence images of EVT-like cells derived from a clonal TS^{blast} line. The cells were stained for HLA-G. Similar results were obtained with three clonal lines derived from TS^{blast} 1.
- (M) Confocal images of ST(3D) cells derived from a clonal TS^{blast} line. The cells were stained for CGB and SDC1. Similar results were obtained with three clonal lines derived from TS^{blast} 1.

The scale bars indicate 100 μm . See also Figure S3 and Table S3.

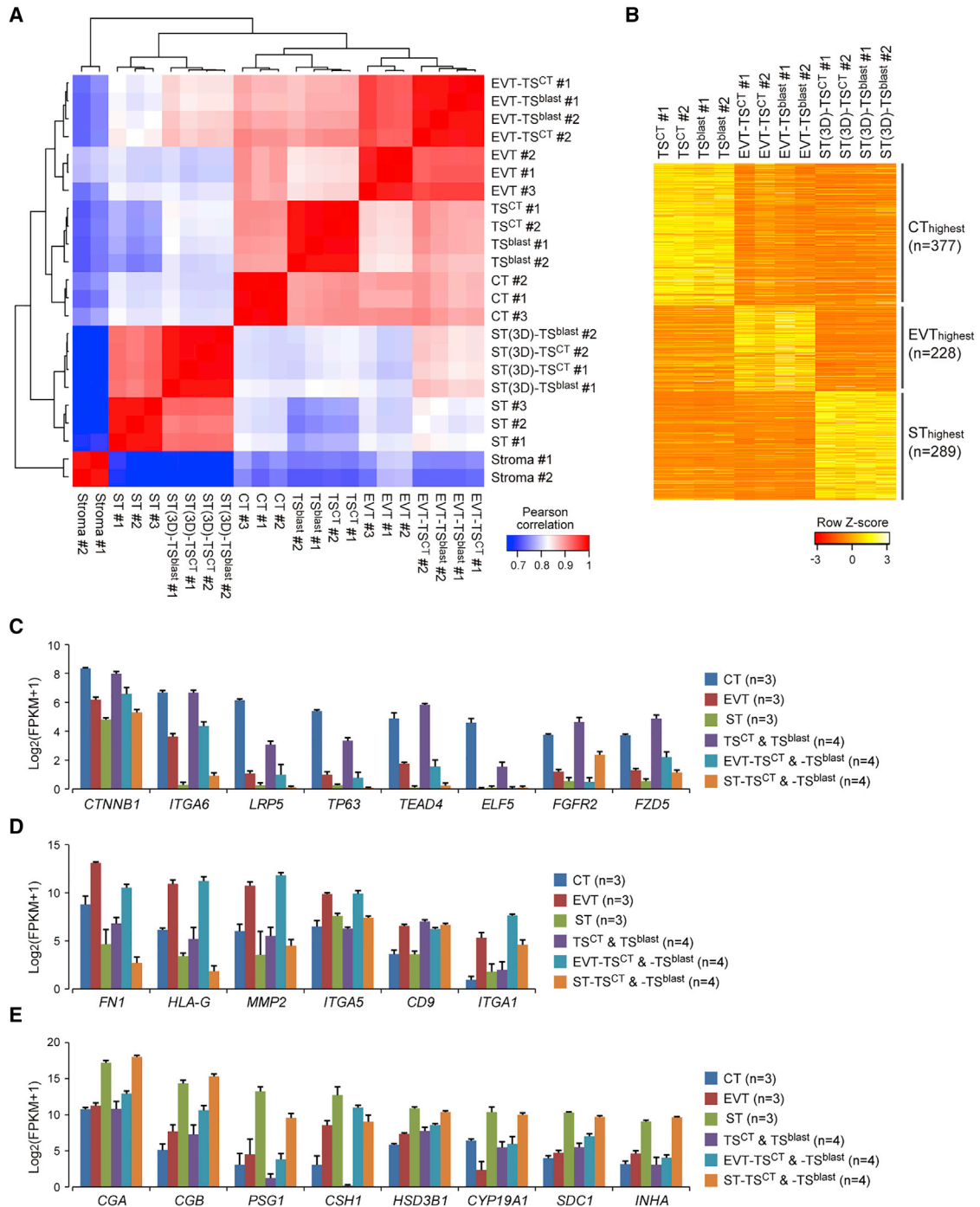


Figure 4. RNA-Seq-Based Transcriptome Profiling of TS^{CT} and TS^{blast} Cells

(A) Heatmap representation of Pearson correlation coefficients between primary and cultured trophoblast cells. Stromal cells derived from human placentas were included for comparison. Differentially expressed genes (adjusted $p < 0.05$, $n = 17,460$) were analyzed.

(B) Expression patterns of CT^{highest}, EVT^{highest}, and ST^{highest} genes in TS^{CT} and TS^{blast} cells and their derivatives. These genes are the same genes as those shown in Figure 1A. Z score-transformed FPKM values are shown.

(C–E) Expression levels of CT (C), EVT (D), and ST markers (E) in primary and cultured trophoblast cells. Data are presented as mean + SD. Note that the data from TS^{CT} and TS^{blast} cells are combined.

See also Figure S4 and Table S1.

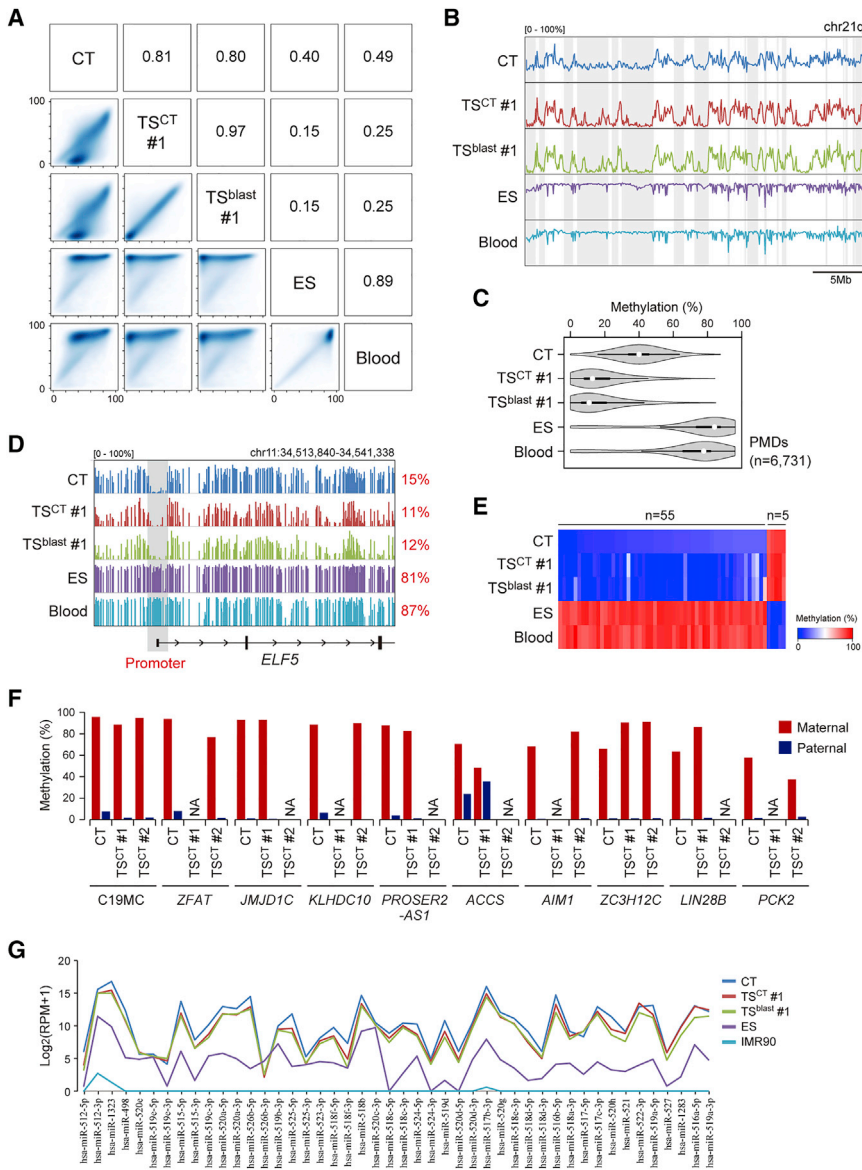


Figure 5. DNA Methylation Profiling of TS^{CT} and TS^{blast} Cells

(A) Heat scatterplots and Pearson correlation coefficients for comparison of DNA methylation levels between CT, TS^{CT}, TS^{blast}, human ES, and cord blood cells. WGBS data were analyzed using 10-kb windows. Publicly available data were used for CT cells (Hamada et al., 2016), human ESCs (Lister et al., 2011), and cord blood cells (Okae et al., 2014).

(B) DNA methylation levels across the long arm of chromosome 21. The vertical axis indicates the methylation level (percent). PMDs defined in a previous study (Schroeder et al., 2013) are shown in gray.

(C) Violin plots of DNA methylation levels of PMDs. Thin and thick lines are boxplots, and white dots indicate the median.

(D) DNA methylation patterns at the *ELF5* locus. The *ELF5* promoter region is highlighted in gray, and its methylation levels are indicated on the right.

(E) DNA methylation levels of promoters differentially methylated between CT cells and embryonic cells. We analyzed 55 promoters hypomethylated (<20%) in CT cells and hypermethylated (>80%) in ESCs and blood cells and 5 promoters with the opposite pattern.

(F) Allelic DNA methylation levels of placenta-specific gDMRs in TS^{CT} cells. Except for the ACCS DMR, maternal allele-specific methylation was maintained. The allelic DNA methylation data for CT cells were obtained in our previous study (Hamada et al., 2016). NA, not analyzed because of the lack of informative SNPs.

(G) Expression levels of C19MC miRNAs in primary and cultured trophoblast cells. Publicly available data for human ESCs (GEO: GSM438362) and IMR90 cells (GEO: GSM438364) were also analyzed.

See also Figure S5 and Tables S4, S5, and S6.

(30%–70%) in CT (33 of 33), TS^{CT} (26 of 33), and TS^{blast} cells (24 of 33) but not in ESCs (0 of 33) or blood cells (0 of 33). We analyzed allele-specific DNA methylation in two TS^{CT} cell lines using targeted bisulfite sequencing (see STAR Methods for details). The allelic methylation patterns were successfully obtained for ten placenta-specific gDMRs, and nine of them maintained maternal allele-specific DNA methylation in TS^{CT} cells (Figure 5F). We did not analyze the allelic DNA methylation patterns in TS^{blast} cells because the maternal genotype was not available. However, nine of the ten gDMRs maintained intermediate methylation levels (30%–70%) in TS^{blast} cells (Figure 5S5C), implying that their imprinted methylation patterns might be similar in TS^{CT} and TS^{blast} cells. Among the genes shown in Figure 5F, four genes had SNPs available for allelic expression analysis. The four genes showed similar allelic expression patterns in primary CT and TS^{CT} cells (Figure 5S5D). We also found that the expression levels of X-linked genes were comparable between male and fe-

male TS cells and that *XIST* was expressed only in female TS cells (Figure 5S5E), suggesting that one X chromosome may be inactivated in female TS cells.

Among the gDMRs shown in Figure 5F, the chromosome 19 microRNA (miRNA) cluster (C19MC) differentially methylated region (DMR) regulates the imprinted expression of C19MC in the placenta (Noguer-Dance et al., 2010). C19MC miRNAs are almost exclusively expressed in the placenta (Bortolin-Cavallé et al., 2009). We performed miRNA sequencing in CT, TS^{CT}, and TS^{blast} cells and compared the data with those of human ESCs (GEO: GSM438362) and IMR90 cells (GEO: GSM438364). We found that C19MC miRNAs were highly expressed in CT, TS^{CT}, and TS^{blast} cells, weakly expressed in human ESCs, and almost absent in IMR90 cells (Figure 5G; Table S6). In addition, TS^{CT} and TS^{blast} cells had global miRNA expression patterns more similar to CT cells ($R > 0.84$) than to ESCs or IMR90 cells ($R < 0.64$) (Figure 5S5F).

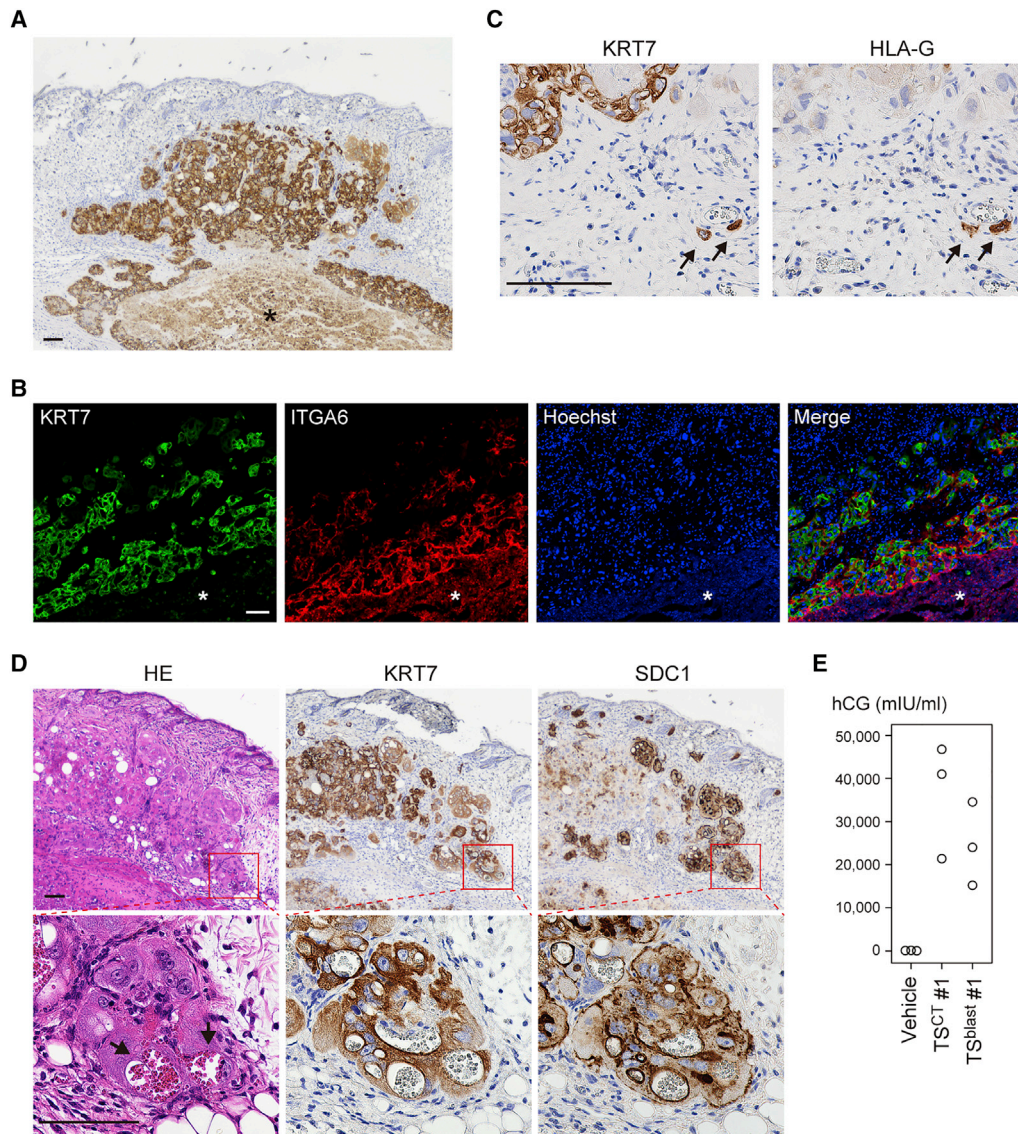


Figure 6. Engraftment of TS^{CT} and TS^{blast} Cells into NOD-SCID Mice

(A) Immunohistochemical staining of KRT7 in a TS-derived lesion. The nuclei were stained with hematoxylin. The injected cells invaded the dermal and subcutaneous tissues. Similar results were obtained with three TS^{CT} 1- and three TS^{blast} 1-derived lesions. Asterisk, necrotic area.

(B) Immunofluorescence images of a TS-derived lesion. The lesion was stained for KRT7 and ITGA6, and the nuclei were stained with Hoechst 33258. Similar results were obtained with two TS^{CT} 1- and two TS^{blast} 1-derived lesions. Asterisk, necrotic area.

(C) Immunohistochemical staining of KRT7 and HLA-G in a TS-derived lesion. Arrows indicate HLA-G-positive trophoblast cells. HLA-G-positive cells were observed in two TS^{CT} 1- and two TS^{blast} 1-derived lesions.

(D) H&E and immunohistochemical staining of KRT7 and SDC1 in a TS-derived lesion. Some SDC1-positive trophoblast cells contained blood-filled lacunae (arrows). In addition to trophoblast cells, some mouse hair follicle cells were SDC1-positive. Similar results were obtained with three TS^{CT} 1- and three TS^{blast} 1-derived lesions.

(E) Serum hCG levels. NOD-SCID mice injected with TS cells or vehicle were analyzed on day 7.

The scale bars indicate 100 μ m.

Engraftment of Human TS Cells into NOD-SCID Mice

To assess the *in vivo* potential of TS^{CT} and TS^{blast} cells, we subcutaneously injected them (1×10^7) into non-obese diabetic (NOD)-severe combined immunodeficiency (SCID) mice. The injected cells formed \sim 5-mm lesions by day 7 and were then gradually resorbed. Immunohistochemical staining of KRT7 revealed that the injected cells invaded the dermal and subcutaneous tis-

sues (Figure 6A). The central area of the lesions was necrotic and surrounded by ITGA6-positive CT-like cells (Figure 6B). We identified EVT-like cells migrating as single cells (Figure 6C), but they were few in number. We analyzed 14 sections from four lesions, and only 4–18 HLA-G-positive cells were observed per section. SDC1-positive ST-like cells were observed at the peripheral region of the lesions (Figure 6D). Interestingly, some of the

ST-like cells contained blood-filled *lacunae*, reminiscent of primitive ST cells that form during implantation, invade the maternal endometrium and erode maternal sinusoids (James et al., 2012). We also found that the host mouse serum contained a substantial amount of hCG (Figure 6E). Although a villous-like structure was not observed, these data suggest that TS cells injected into NOD-SCID mice mimic some key features of trophoblast invasion during implantation.

DISCUSSION

Lee et al. (2016) proposed robust criteria for human trophoblast cells: expression of protein markers (GATA3, KRT7, and TFAPC2), HLA class I profile, hypomethylation of the *ELF5* promoter, and expression of C19MC. Although we did not perform immunostaining for TFAPC2, we confirmed that TS^{CT} and TS^{blast} cells meet all other criteria, and, furthermore, our RNA-seq clearly showed high expression of *TFAPC2* in CT, TS^{CT}, and TS^{blast} cells (FPKM, 50–80). In addition to the above, TS^{CT} and TS^{blast} cells had the ability to proliferate for more than 150 population doublings and differentiate into EVT- and ST-like cells. The transcriptome and methylome analyses indicate that TS^{CT} and TS^{blast} cells maintain many properties unique to trophoblast cells. Furthermore, TS^{CT} and TS^{blast} cells injected into immunodeficient mice mimicked some key features of trophoblast invasion during implantation. For ethical reasons, we could not examine whether TS^{CT} and TS^{blast} cells can contribute to all trophoblast subtypes after blastocyst injection. Nonetheless, our comprehensive data strongly suggest that TS^{CT} and TS^{blast} cells are human TS cells.

Among various EVT subtypes, TS-derived EVT-like cells may correspond to EVT cells in distal cell columns for the following reasons. First, EVT-like cells and primary EVT cells had very similar transcriptome profiles. We isolated primary EVT cells from villous tissues, meaning that most of them were derived from cell columns. Second, TS cells differentiating into EVT-like cells gradually lost their proliferation capacity. EVT cells are predominantly nonproliferative *in vivo*, except for those in proximal cell columns, and early postproliferative EVT cells reside in distal cell columns (Bischof and Irminger-Finger, 2005). Third, *CCR1* expression was high in both primary EVT (mean FPKM = 60.3) and EVT-like cells (mean FPKM = 75.4). *CCR1* is specifically expressed in EVT cells in cell columns and a subset of endovascular EVT cells (Sato et al., 2003). Finally, *NCAM1*, a marker of endovascular EVT cells (Burrows et al., 1994), was poorly expressed in primary EVT and EVT-like cells (< 1 FPKM). Unfortunately, little is known about the molecular mechanisms regulating EVT lineage specification, and few reliable markers distinguishing EVT subtypes have been identified. Further *in vivo* and *in vitro* studies are needed to determine whether our TS cells can differentiate into various types of EVT cells.

A number of cell lines, including choriocarcinoma cell lines, immortalized cell lines, and BMP4-treated human ESCs, have been used as models of human trophoblast cells (Gamage et al., 2016). However, such immortalized cell lines (e.g., HTR8/SVneo) and BMP4-treated human ESCs do not meet the criteria proposed by Lee et al. (2016). Some choriocarcinoma cell lines meet those criteria, but their transcriptome profiles are consider-

ably different from those of primary trophoblast cells (Bilban et al., 2010). Most recently, Genbacev et al. (2011) and Zdravkovic et al. (2015) established human trophoblast progenitor cell (TBPC) lines from the chorion and another similar cell line from a human ESC line named UCSFB6. The culture conditions for TBPCs and the UCSFB6-derived cells are substantially different from those for TS^{CT} and TS^{blast} cells, and the only common ingredient is the TGF- β inhibitor SB431542. Although TBPCs and UCSFB6-derived cells express some trophoblast marker proteins, most of the criteria of Lee et al. (2016) have not been tested. In addition, TBPCs and UCSFB6-derived cells have a mesenchymal morphology, whereas TS^{CT} and TS^{blast} cells are epithelial cells. Therefore, TBPCs and UCSFB6-derived cells are clearly different from TS^{CT} and TS^{blast} cells.

We found that activation of Wnt and EGF and inhibition of TGF- β , HDAC, and ROCK are important to derive TS^{CT} and TS^{blast} cells. In contrast, for the derivation of mouse TS cells, activation of FGF and TGF- β and inhibition of Wnt and ROCK are important (Latos and Hemberger, 2016; Ohinata and Tsukiyama, 2014). Hence, TGF- β and Wnt signaling seem to have opposite roles in human and mouse TS cells. Furthermore, although FGFR2c and FGF4 are essential for the maintenance of mouse TS cells (Arman et al., 1998; Tanaka et al., 1998), *FGFR2c* expression was negligible in human CT, TS^{CT}, and TS^{blast} cells. In addition, although FGFR2 protein is highly expressed in mouse blastocysts, it is absent in human blastocysts (Kunath et al., 2014). Therefore, FGFR2c-mediated FGF signaling may be dispensable for the proliferation of human trophoblast cells. There are marked differences between human and mouse placental development (Rossant and Tam, 2017). In mice, the polar trophoderm forms the ExE and ectoplacental cone (EPC) after implantation. Multipotent trophoblast cells are maintained in the ExE, which depends on FGF ligands secreted by the epiblast. In humans, the trophoderm gives rise to primitive CT and ST cells. Primitive ST cells invade the maternal endometrium, and then primitive CT cells penetrate the primitive ST cells to form primary villi (James et al., 2012). Importantly, ExE- and EPC-like structures do not form, and the interaction between epiblast and trophoblast cells is transient in human embryos. Therefore, it is reasonable that human and mouse TS cells require different signaling environments.

The transcription factor networks may also be different between human and mouse TS cells. We found that some key transcription factors controlling mouse TS cell self-renewal were poorly expressed in human trophoblast cells. Most strikingly, *EOMES* was undetectable in CT, TS^{CT}, and TS^{blast} cells. Consistent with this, *EOMES* protein is completely absent in human blastocysts (Blakeley et al., 2015). Thus, *EOMES* may be dispensable for the proliferation of human trophoblast cells both *in vivo* and *in vitro*. The expression levels of *ESRRB* and *SOX2* were also very low (< 0.1 FPKM) in CT, TS^{CT}, and TS^{blast} cells. In mouse TS cells, *Esrrb* and *Sox2* are thought to be the primary targets of the FGFR2c-mediated FGF signaling (Latos et al., 2015), and sustained expression of *Esrrb* and *Sox2* supports their FGF-independent self-renewal (Adachi et al., 2013). The lack of *FGFR2c* expression in CT, TS^{CT}, and TS^{blast} cells is consistent with the very low expression of *ESRRB* and *SOX2*. Furthermore, we found that *CDX2* expression was very low (< 0.1 FPKM) in TS^{CT} and TS^{blast} cells. *CDX2* expression was

also low in CT cells (average FPKM = 0.41). Interestingly, CDX2 expression and localization are dynamic in human preimplantation embryos. Its expression starts after blastocyst formation, and the protein is localized in the nuclei of TE cells (Niakan and Eggan, 2013). However, CDX2 is then downregulated and relocalized to the cytoplasm in human peri-implantation embryos (Chen et al., 2009). Thus, further studies are needed to determine whether CDX2 is functional in human trophoblast lineages.

We were unable to derive human TS cells from CT cells isolated from term placentas. Previous studies suggest that there may be three CT subtypes in the human placenta: ST progenitors, EVT progenitors, and bipotent cells (James et al., 2012). We speculate that the bipotent cells might serve as the source of TS^{CT} cells and be lost during or after the second trimester of pregnancy. CT cells in the first-trimester placenta have the capacity to generate new villi, suggesting that trunk CT cells may be a stem cell source (Castellucci et al., 2000). CT cells in the proximal region of cell columns might also contain bipotent stem cells because they are highly proliferative and can contribute to EVT cells. Attempts to derive TS^{CT} cells from CT cells in various parts of the placenta may help to identify the location of bipotent trophoblast cells. Future studies identifying CT subpopulations and their specific markers are important to identify the source of TS^{CT} cells.

In conclusion, we have established human TS cells from CT cells and blastocysts, which provides a powerful tool for molecular and functional characterization of human trophoblast cells. Furthermore, our culture system for human TS cells is potentially useful for understanding the pathogenesis of developmental disorders with trophoblast defects, such as miscarriage, pre-eclampsia, and intrauterine growth restriction.

STAR★METHODS

Detailed methods are provided in the online version of this paper and include the following:

- **KEY RESOURCES TABLE**
- **CONTACT FOR REAGENT AND RESOURCE SHARING**
- **EXPERIMENTAL MODEL AND SUBJECT DETAILS**
 - Human samples
 - Animal care and use
- **METHOD DETAILS**
 - Experimental design
 - Isolation of trophoblast and stromal cells
 - Culture of TS^{CT}, TS^{blast}, and stromal cells
 - Differentiation of TS^{CT} and TS^{blast} cells
 - RNA-seq
 - MiRNA-seq
 - WGBS
 - Targeted bisulfite sequencing (BS)
 - Allelic expression analysis
 - Combined bisulfite restriction analysis (COBRA)
 - Immunostaining
 - Flow cytometry
 - Measurement of hCG
 - Quantitative real-time PCR analysis
 - Chromosome analysis
 - Engraftment of TS cells into NOD-SCID mice

- Annotations of genomic regions and differentially expressed genes
- Graphical presentation
- External data
- **QUANTIFICATION AND STATISTICAL ANALYSES**
- **DATA AND SOFTWARE AVAILABILITY**

SUPPLEMENTAL INFORMATION

Supplemental Information includes five figures, six tables, and one methods file and can be found with this article online at <https://doi.org/10.1016/j.stem.2017.11.004>.

AUTHOR CONTRIBUTIONS

Conceptualization, H.O. and T.A.; Investigation, H.O., H.H., S.T., K.S., and Y.K.; Formal Analysis, H.O., H.T., T.S., and M.S.; Writing – Original Draft, H.O., H.S., and T.A.; Writing – Review & Editing, H.O., H.S., and T.A.; Funding Acquisition, H.O., M.S., H.S., and T.A.

ACKNOWLEDGMENTS

We thank all individuals and their families who participated in this study. We also thank H. Yoshida, H. Kikuchi, K. Nakayama, R. Funayama, M. Tsuda, M. Kikuchi, M. Nakagawa, and K. Kuroda for technical assistance and R.M. John and N. Ishii for support and valuable suggestions. We are also grateful to the Biomedical Research Core of Tohoku University Graduate School of Medicine for technical support. This work was supported by the Core Research for Evolutional Science and Technology (CREST) from the Japan Agency for Medical Research and Development (AMED) (to M.S., H.S., and T.A.). This work was also supported by Grants-in-Aid for Scientific Research (KAKENHI) (17H04335) and the Smoking Research Foundation (to T.A.) and KAKENHI (26112502 and 15K10657) (to H.O.).

Received: May 16, 2017
 Revised: September 20, 2017
 Accepted: November 2, 2017
 Published: December 14, 2017

REFERENCES

- Adachi, K., Nikaïdo, I., Ohta, H., Ohtsuka, S., Ura, H., Kadota, M., Wakayama, T., Ueda, H.R., and Niwa, H. (2013). Context-dependent wiring of Sox2 regulatory networks for self-renewal of embryonic and trophoblast stem cells. *Mol. Cell* 52, 380–392.
- Arman, E., Haffner-Krausz, R., Chen, Y., Heath, J.K., and Lonai, P. (1998). Targeted disruption of fibroblast growth factor (FGF) receptor 2 suggests a role for FGF signaling in pregastrulation mammalian development. *Proc. Natl. Acad. Sci. USA* 95, 5082–5087.
- Bilban, M., Tauber, S., Haslinger, P., Pollheimer, J., Saleh, L., Pehamberger, H., Wagner, O., and Knöfler, M. (2010). Trophoblast invasion: assessment of cellular models using gene expression signatures. *Placenta* 31, 989–996.
- Bischof, P., and Irminger-Finger, I. (2005). The human cytotrophoblastic cell, a mononuclear chameleon. *Int. J. Biochem. Cell Biol.* 37, 1–16.
- Blakeley, P., Fogarty, N.M., del Valle, I., Wamaitha, S.E., Hu, T.X., Elder, K., Snell, P., Christie, L., Robson, P., and Niakan, K.K. (2015). Defining the three cell lineages of the human blastocyst by single-cell RNA-seq. *Development* 142, 3151–3165.
- Bortolin-Cavaillé, M.L., Dance, M., Weber, M., and Cavaillé, J. (2009). C19MC microRNAs are processed from introns of large Pol-II, non-protein-coding transcripts. *Nucleic Acids Res.* 37, 3464–3473.
- Burrows, T.D., King, A., and Loke, Y.W. (1994). Expression of adhesion molecules by endovascular trophoblast and decidual endothelial cells: implications for vascular invasion during implantation. *Placenta* 15, 21–33.

- Castellucci, M., Kosanke, G., Verdenelli, F., Huppertz, B., and Kaufmann, P. (2000). Villous sprouting: fundamental mechanisms of human placental development. *Hum. Reprod. Update* 6, 485–494.
- Chen, A.E., Egli, D., Niakan, K., Deng, J., Akutsu, H., Yamaki, M., Cowan, C., Fitz-Gerald, C., Zhang, K., Melton, D.A., and Eggan, K. (2009). Optimal timing of inner cell mass isolation increases the efficiency of human embryonic stem cell derivation and allows generation of sibling cell lines. *Cell Stem Cell* 4, 103–106.
- Cierna, Z., Varga, I., Danihel, L., Jr., Kuracinova, K., Janegova, A., and Danihel, L. (2016). Intermediate trophoblast—A distinctive, unique and often unrecognized population of trophoblastic cells. *Ann. Anat* 204, 45–50.
- Cohen, C.J., Rebollo, R., Babovic, S., Dai, E.L., Robinson, W.P., and Mager, D.L. (2011). Placenta-specific expression of the interleukin-2 (IL-2) receptor β subunit from an endogenous retroviral promoter. *J. Biol. Chem.* 286, 35543–35552.
- Court, F., Tayama, C., Romanelli, V., Martin-Trujillo, A., Iglesias-Platas, I., Okamura, K., Sugahara, N., Simón, C., Moore, H., Harness, J.V., et al. (2014). Genome-wide parent-of-origin DNA methylation analysis reveals the intricacies of human imprinting and suggests a germline methylation-independent mechanism of establishment. *Genome Res.* 24, 554–569.
- Du, Y., Zhang, J., Wang, H., Yan, X., Yang, Y., Luo, X., Chen, Y., Duan, T., and Ma, D. (2011). Hypomethylated DSCR4 is a placenta-derived epigenetic marker for trisomy 21. *Prenat. Diagn.* 31, 207–214.
- Fatehullah, A., Tan, S.H., and Barker, N. (2016). Organoids as an in vitro model of human development and disease. *Nat. Cell Biol.* 18, 246–254.
- Fock, V., Plessl, K., Draxler, P., Otti, G.R., Fiala, C., Knöfler, M., and Pollheimer, J. (2015). Neuregulin-1-mediated ErbB2–ErbB3 signalling protects human trophoblasts against apoptosis to preserve differentiation. *J. Cell Sci.* 128, 4306–4316.
- Gamage, T.K., Chamley, L.W., and James, J.L. (2016). Stem cell insights into human trophoblast lineage differentiation. *Hum. Reprod. Update* 23, 77–103.
- Genbacev, O., Donne, M., Kapidzic, M., Gormley, M., Lamb, J., Gilmore, J., Larocque, N., Goldfien, G., Zdravkovic, T., McMaster, M.T., and Fisher, S.J. (2011). Establishment of human trophoblast progenitor cell lines from the chorion. *Stem Cells* 29, 1427–1436.
- Hamada, H., Okae, H., Toh, H., Chiba, H., Hiura, H., Shirane, K., Sato, T., Suyama, M., Yaegashi, N., Sasaki, H., and Arima, T. (2016). Allele-Specific Methylome and Transcriptome Analysis Reveals Widespread Imprinting in the Human Placenta. *Am. J. Hum. Genet.* 99, 1045–1058.
- Hemberger, M., Udayashankar, R., Tesar, P., Moore, H., and Burton, G.J. (2010). ELF5-enforced transcriptional networks define an epigenetically regulated trophoblast stem cell compartment in the human placenta. *Hum. Mol. Genet.* 19, 2456–2467.
- Herwig, R., Hardt, C., Lienhard, M., and Kamburov, A. (2016). Analyzing and interpreting genome data at the network level with ConsensusPathDB. *Nat. Protoc.* 11, 1889–1907.
- Hsu, Y.C., Li, L., and Fuchs, E. (2014). Emerging interactions between skin stem cells and their niches. *Nat. Med.* 20, 847–856.
- James, J.L., Carter, A.M., and Chamley, L.W. (2012). Human placentation from nidation to 5 weeks of gestation. Part I: What do we know about formative placental development following implantation? *Placenta* 33, 327–334.
- King, A., Thomas, L., and Bischof, P. (2000). Cell culture models of trophoblast II: trophoblast cell lines—a workshop report. *Placenta* 21, S113–S119.
- Kozomara, A., and Griffiths-Jones, S. (2014). miRBase: annotating high confidence microRNAs using deep sequencing data. *Nucleic Acids Res.* 42, D68–D73.
- Krueger, F., and Andrews, S.R. (2011). Bismark: a flexible aligner and methylation caller for Bisulfite-Seq applications. *Bioinformatics* 27, 1571–1572.
- Kunath, T., Yamanaka, Y., Detmar, J., MacPhee, D., Caniggia, I., Rossant, J., and Jurisicova, A. (2014). Developmental differences in the expression of FGF receptors between human and mouse embryos. *Placenta* 35, 1079–1088.
- Latos, P.A., and Hemberger, M. (2016). From the stem of the placental tree: trophoblast stem cells and their progeny. *Development* 143, 3650–3660.
- Latos, P.A., Goncalves, A., Oxley, D., Mohammed, H., Turro, E., and Hemberger, M. (2015). Fgf and Esrrb integrate epigenetic and transcriptional networks that regulate self-renewal of trophoblast stem cells. *Nat. Commun.* 6, 7776.
- Lee, C.Q., Gardner, L., Turco, M., Zhao, N., Murray, M.J., Coleman, N., Rossant, J., Hemberger, M., and Moffett, A. (2016). What Is Trophoblast? A Combination of Criteria Define Human First-Trimester Trophoblast. *Stem Cell Reports* 6, 257–272.
- Lister, R., Pelizzola, M., Kida, Y.S., Hawkins, R.D., Nery, J.R., Hon, G., Antosiewicz-Bourget, J., O'Malley, R., Castanon, R., Klugman, S., et al. (2011). Hotspots of aberrant epigenomic reprogramming in human induced pluripotent stem cells. *Nature* 471, 68–73.
- Love, M.I., Huber, W., and Anders, S. (2014). Moderated estimation of fold change and dispersion for RNA-seq data with DESeq2. *Genome Biol.* 15, 550.
- Macaulay, E.C., Weeks, R.J., Andrews, S., and Morison, I.M. (2011). Hypomethylation of functional retrotransposon-derived genes in the human placenta. *Mamm. Genome* 22, 722–735.
- McConkey, C.A., Delorme-Axford, E., Nickerson, C.A., Kim, K.S., Sadovsky, Y., Boyle, J.P., and Coyne, C.B. (2016). A three-dimensional culture system recapitulates placental syncytiotrophoblast development and microbial resistance. *Sci. Adv.* 2, e1501462.
- Miller, R.K., Genbacev, O., Turner, M.A., Aplin, J.D., Caniggia, I., and Huppertz, B. (2005). Human placental explants in culture: approaches and assessments. *Placenta* 26, 439–448.
- Miura, F., Enomoto, Y., Dairiki, R., and Ito, T. (2012). Amplification-free whole-genome bisulfite sequencing by post-bisulfite adaptor tagging. *Nucleic Acids Res.* 40, e136.
- Moffett, A., and Loke, C. (2006). Immunology of placentation in eutherian mammals. *Nat. Rev. Immunol.* 6, 584–594.
- Moser, G., Gauster, M., Orendi, K., Glasner, A., Theuerkauf, R., and Huppertz, B. (2010). Endoglandular trophoblast, an alternative route of trophoblast invasion? Analysis with novel confrontation co-culture models. *Hum. Reprod.* 25, 1127–1136.
- Niakan, K.K., and Eggan, K. (2013). Analysis of human embryos from zygote to blastocyst reveals distinct gene expression patterns relative to the mouse. *Dev. Biol.* 375, 54–64.
- Noguer-Dance, M., Abu-Amero, S., Al-Khtib, M., Lefèvre, A., Coullin, P., Moore, G.E., and Cavallé, J. (2010). The primate-specific microRNA gene cluster (C19MC) is imprinted in the placenta. *Hum. Mol. Genet.* 19, 3566–3582.
- Norwitz, E.R. (2006). Defective implantation and placentation: laying the blueprint for pregnancy complications. *Reprod. Biomed. Online* 13, 591–599.
- Ohinata, Y., and Tsukiyama, T. (2014). Establishment of trophoblast stem cells under defined culture conditions in mice. *PLoS ONE* 9, e107308.
- Okae, H., Chiba, H., Hiura, H., Hamada, H., Sato, A., Utsunomiya, T., Kikuchi, H., Yoshida, H., Tanaka, A., Suyama, M., and Arima, T. (2014). Genome-wide analysis of DNA methylation dynamics during early human development. *PLoS Genet.* 10, e1004868.
- Pröll, J., Bensussan, A., Goffin, F., Foidart, J.M., Berrebi, A., and Le Bouteiller, P. (2000). Tubal versus uterine placentation: similar HLA-G expressing extravillous cytotrophoblast invasion but different maternal leukocyte recruitment. *Tissue Antigens* 56, 479–491.
- Rawn, S.M., and Cross, J.C. (2008). The evolution, regulation, and function of placenta-specific genes. *Annu. Rev. Cell Dev. Biol.* 24, 159–181.
- Reis-Filho, J.S., Simpson, P.T., Martins, A., Preto, A., Gartner, F., and Schmitt, F.C. (2003). Distribution of p63, cytokeratins 5/6 and cytokeratin 14 in 51 normal and 400 neoplastic human tissue samples using TARP-4 multi-tumor tissue microarray. *Virchows Arch* 443, 122–132.
- Robinson, W.P., and Price, E.M. (2015). The human placental methylome. *Cold Spring Harb. Perspect. Med.* 5, a023044.

- Robinson, J.T., Thorvaldsdóttir, H., Winckler, W., Guttman, M., Lander, E.S., Getz, G., and Mesirov, J.P. (2011). Integrative genomics viewer. *Nat. Biotechnol.* *29*, 24–26.
- Rossant, J., and Tam, P.P. (2017). New Insights into Early Human Development: Lessons for Stem Cell Derivation and Differentiation. *Cell Stem Cell* *20*, 18–28.
- Sato, Y., Higuchi, T., Yoshioka, S., Tatsumi, K., Fujiwara, H., and Fujii, S. (2003). Trophoblasts acquire a chemokine receptor, CCR1, as they differentiate towards invasive phenotype. *Development* *130*, 5519–5532.
- Schroeder, D.I., Blair, J.D., Lott, P., Yu, H.O., Hong, D., Cray, F., Ashwood, P., Walker, C., Korf, I., Robinson, W.P., and LaSalle, J.M. (2013). The human placenta methylome. *Proc. Natl. Acad. Sci. USA* *110*, 6037–6042.
- Soncin, F., Natale, D., and Parast, M.M. (2015). Signaling pathways in mouse and human trophoblast differentiation: a comparative review. *Cell. Mol. Life Sci.* *72*, 1291–1302.
- Strauss, J.F., 3rd, Kido, S., Sayegh, R., Sakuragi, N., and Gáfvels, M.E. (1992). The cAMP signalling system and human trophoblast function. *Placenta* *13*, 389–403.
- Tanaka, S., Kunath, T., Hadjantonakis, A.K., Nagy, A., and Rossant, J. (1998). Promotion of trophoblast stem cell proliferation by FGF4. *Science* *282*, 2072–2075.
- Trapnell, C., Roberts, A., Goff, L., Pertea, G., Kim, D., Kelley, D.R., Pimentel, H., Salzberg, S.L., Rinn, J.L., and Pachter, L. (2012). Differential gene and transcript expression analysis of RNA-seq experiments with TopHat and Cufflinks. *Nat. Protoc.* *7*, 562–578.
- Vogt, J., Traynor, R., and Sapkota, G.P. (2011). The specificities of small molecule inhibitors of the TGF β and BMP pathways. *Cell. Signal.* *23*, 1831–1842.
- Windsperger, K., Dekan, S., Pils, S., Golletz, C., Kunihs, V., Fiala, C., Kristiansen, G., Knöfler, M., and Pollheimer, J. (2017). Extravillous trophoblast invasion of venous as well as lymphatic vessels is altered in idiopathic, recurrent, spontaneous abortions. *Hum. Reprod.* *32*, 1208–1217.
- Zdravkovic, T., Nazor, K.L., Larocque, N., Gormley, M., Donne, M., Hunkapillar, N., Giritharan, G., Bernstein, H.S., Wei, G., Hebrok, M., et al. (2015). Human stem cells from single blastomeres reveal pathways of embryonic or trophoblast fate specification. *Development* *142*, 4010–4025.

STAR★METHODS

KEY RESOURCES TABLE

REAGENT or RESOURCE	SOURCE	IDENTIFIER
Antibodies		
PE-conjugated anti-ITGA6	Miltenyi Biotec	Cat#130-097-246, RRID:AB_2658554
PE-conjugated anti-HLA-G	Novus Biologicals	Cat#NB500-612, RRID:AB_10000639
PE-conjugated anti-SDC1	Miltenyi Biotec	Cat#130-081-301, RRID:AB_244212
PE-conjugated anti-Thy1	Miltenyi Biotec	Cat#130-095-400, RRID:AB_10839701
FITC-conjugated anti-HLA-ABC	Thermo Fisher Scientific	Cat#11-9983-41, RRID:AB_1633403
Anti-KRT7	Abnova	Cat#MAB11033, RRID: not available
Anti-TP63	Cell Signaling	Cat#13109, RRID: not available
Anti-GATA3	Cell Signaling	Cat#5852, RRID:AB_10835690
Anti-TEAD4	Abcam	Cat#ab58310, RRID:AB_945789
Anti-CDH1	Cell Signaling	Cat#3195, RRID:AB_10694492
Anti-hCG	DAKO	Cat#IS508, RRID: not available
Anti-VIM	Cell Signaling	Cat#5741, RRID:AB_10695459
Anti-HLA-G	MBL	Cat#K0125-3, RRID:AB_592237
Alexa Fluor 488-conjugated anti-rabbit IgG	Cell Signaling	Cat#4412, RRID:AB_1904025
Alexa Fluor 488-conjugated anti-mouse IgG	Cell Signaling	Cat#4408, RRID:AB_10694704
Alexa Fluor 555-conjugated anti-rabbit IgG	Cell Signaling	Cat#4413, RRID:AB_10694110
Alexa Fluor 555-conjugated anti-mouse IgG	Cell Signaling	Cat#4409, RRID:AB_1904022
HRP-conjugated anti-rabbit IgG	Cell Signaling	Cat#7074, RRID:AB_209923
HRP-conjugated anti-mouse IgG	Cell Signaling	Cat#7076, RRID:AB_330924
FITC-conjugated mouse IgG2a	Thermo Fisher Scientific	Cat#11-4724, RRID:AB_1963642
PE-conjugated mouse IgG1	R&D	Cat#IC002P, RRID:AB_357242
PE-conjugated rat IgG2A	R&D	Cat#IC006P, RRID:AB_357256
Chemicals, Peptides, and Recombinant Proteins		
TrypLE	Thermo Fisher Scientific	Cat#12604021
Accumax	Innovative Cell Tech	Cat#AM105-500
Percoll	GE Healthcare Life Sciences	Cat#17-5445-02
Col IV	Corning	Cat#354233
DMEM/F12	Wako	Cat#048-29785
DMEM	Thermo Fisher Scientific	Cat#11995065
2-Mercaptoethanol	Thermo Fisher Scientific	Cat#21985023
FBS	Thermo Fisher Scientific	Cat#16141-079
Penicillin-Streptomycin	Thermo Fisher Scientific	Cat#15140122
BSA	Wako	Cat#017-22231
ITS-X supplement	Wako	Cat#094-06761
L-ascorbic acid	Wako	Cat#013-12061
EGF	Wako	Cat#053-07871
CHIR99021	Wako	Cat#038-23101
A83-01	Wako	Cat#035-24113
SB431542	Wako	Cat#031-24291
VPA	Wako	Cat#227-01071
Y27632	Wako	Cat#257-00511
FGF10	Wako	Cat#060-04401
HGF	Wako	Cat#082-08721
NOG	Wako	Cat#146-08991

(Continued on next page)

Continued

REAGENT or RESOURCE	SOURCE	IDENTIFIER
NRG1	Cell Signaling	Cat# 5218SC
TSA	Wako	Cat#203-17561
SAHA	Cell Signaling	Cat#12520S
Forskolin	Wako	Cat#067-02191
Matrigel	Corning	Cat#354234
Sodium pyruvate	Thermo Fisher Scientific	Cat# 11360070
L-glutamine	Thermo Fisher Scientific	Cat#25030
Cell Banker 1	Nippon Zenyaku Kogyo	Cat#CB011
KnockOut Serum Replacement	Thermo Fisher Scientific	Cat#10828028
Tyrode's solution	Gonagen Medikal	Cat#99252
Critical Commercial Assays		
EasySep PE selection kit	StemCell Technologies	Cat#18551
hCG ELISA kit	Abnova	Cat# KA4005
Deposited Data		
Sequencing data of EVT, ST, and stromal cells	This paper	JGA: JGA00000000074
Sequencing data of TS ^{CT} cells	This paper	JGA: JGA00000000117
Sequencing data of TS ^{blast} cells	This paper	JGA: JGA00000000122
RNA-seq of CT cells	(Hamada et al., 2016)	JGA: JGAX00000007522, JGAX00000007532, and JGAX00000007538
WGBS of CT cells	(Hamada et al., 2016)	JGA: JGAX00000007488
WGBS of cord blood cells	(Okae et al., 2014)	DDBJ: DRX036834-8
WGBS of human ESCs	(Lister et al., 2011)	GEO:GSM706059
miRNA-seq of human ESCs	http://www.roadmapepigenomics.org/	GEO:GSM438362
miRNA-seq of IMR90 cells	http://www.roadmapepigenomics.org/	GEO:GSM438364
Experimental Models: Cell Lines		
See Table S3 for TS ^{CT} and TS ^{blast} cell lines derived in this paper	N/A	N/A
Experimental Models: Organisms/Strains		
Mouse: NOD-SCID	CLEA Japan	NOD/ShiJic-scidJcl
Oligonucleotides		
See Methods S1 for primer sequences	N/A	N/A
Software and Algorithms		
Bismark (v0.9.0)	https://www.bioinformatics.babraham.ac.uk/projects/bismark	N/A
Bowtie2 (v2.1.0)	http://bowtie-bio.sourceforge.net/bowtie2/index.shtml	N/A
ConsensusPathDB (v31)	http://cpdb.molgen.mpg.de/	N/A
Cufflinks (v2.2.1)	http://cole-trapnell-lab.github.io/cufflinks/	N/A
DESeq2 (v1.12.4)	https://bioconductor.org/packages/release/bioc/html/DESeq2.html	N/A
FlowJo software (v10)	Tommy Digital	N/A
GSEA (v3.0)	https://www.broadinstitute.org/gsea	N/A
IGV	http://software.broadinstitute.org/software/igv/	N/A
Vioplot package	http://neoscience.org/~plex/	N/A
R (v3.3.1)	http://www.R-project.org/	N/A
TopHat (v2.0.13)	http://ccb.jhu.edu/software/tophat/index.shtml	N/A
UCSC Genome Browser	https://genome.ucsc.edu/	N/A

CONTACT FOR REAGENT AND RESOURCE SHARING

Further information and requests for resources and reagents may be directed to and will be fulfilled by the Lead Contact, Hiroaki Okae (okaehiro@m.tohoku.ac.jp).

EXPERIMENTAL MODEL AND SUBJECT DETAILS

Human samples

Human placentas were obtained from healthy women with signed informed consent of the donors, and the approval of the Ethics Committee of Tohoku University School of Medicine (Research license 2014-1-879). First trimester placentas (6–9 weeks gestation) were obtained from elective termination of pregnancies with live fetuses. Term placentas were obtained after elective caesarean section. Human blastocysts were obtained with signed informed consent of the donors, and the approval of the Ethics Committee of Tohoku University School of Medicine (Research license 2016-1-371), associated hospitals, the Japan Society of Obstetrics and Gynecology and the Ministry of Education, Culture, Sports, Science and Technology (Japan). The sex and developmental stage of each human sample used for the derivation of TS cells are summarized in [Table S3](#). The sample size for each experiment is given in the figure legend. No samples were excluded from any of the experiments.

Animal care and use

Six-week-old male NOD-SCID mice were obtained from CLEA Japan and maintained under specific-pathogen-free conditions. All animal experiments were approved by the Animal Care and Use Committee of Tohoku University (Research license 2015-051) and performed according to the guidelines for animal experiments at Tohoku University.

METHOD DETAILS

Experimental design

At least two biological replicates were performed for each experiment, except for WGBS and miRNA-seq in [Figure 5](#). Randomization and blinding were not performed. No statistical methods were used to predetermine sample size. No data or samples were excluded from any of the experiments.

Isolation of trophoblast and stromal cells

CT, EVT, and stromal cells were isolated from fresh placental tissues as described previously ([Hamada et al., 2016](#)). For first trimester placentas, whole placental villi were cut into small pieces and enzymatically digested three times in a solution containing equal amounts of TrypLE and Accumax for 20 min at 37°C. Pooled cell suspensions were filtered through a 70 μ m mesh filter. CT cells were immunomagnetically purified using the EasySep PE selection kit and a PE-conjugated anti-ITGA6 antibody. EVT and stromal cells were also isolated from first trimester placentas in a similar way using a PE-conjugated anti-HLA-G antibody and a PE-conjugated anti-Thy1 antibody, respectively. For term placentas, about 50 g of placental villous tissue was cut into small pieces, washed with 0.9% saline solution, and enzymatically digested six times as described above. Single-cell suspensions were prepared by filtration, and red blood cells and cell debris were removed using Percoll density gradient (10%–70%) centrifugation. ITGA6-positive CT cells were purified immunomagnetically as described above. The cell purity was evaluated by flow cytometry (FACSARIA II, BD Bioscience, San Jose) and typically exceeded 90%.

ST cells shed from first trimester placentas, which are known as syncytial sprouts, were collected by sequential filtration as follows. A fresh placental sample was placed in a 50 mL tube containing 30–40 mL of 0.9% saline solution, and the tube was gently inverted several times. The placental sample and saline solution were passed through a 100 μ m mesh filter to remove placental villi and large debris. The flowthrough was next passed through a 40 μ m mesh filter and the filter was washed with 0.9% saline solution. Finally, we collected ST cells remaining on the 40 μ m mesh filter. The cell viability was assessed by propidium iodide exclusion and ranged from 80% to 90%.

Culture of TS^{CT}, TS^{blast}, and stromal cells

A 6-well plate was coated with 5 μ g/ml Col IV at 37°C for at least one hour. CT cells were seeded in the 6-well plate at a density of $0.5\text{--}1 \times 10^6$ cells per well and cultured in 2 mL of TS medium [DMEM/F12 supplemented with 0.1 mM 2-mercaptoethanol, 0.2% FBS, 0.5% Penicillin-Streptomycin, 0.3% BSA, 1% ITS-X supplement, 1.5 μ g/ml L-ascorbic acid, 50 ng/ml EGF, 2 μ M CHIR99021, 0.5 μ M A83-01, 1 μ M SB431542, 0.8 mM VPA and 5 μ M Y27632]. Cells were cultured at 37°C in 5% CO₂ and the culture medium was replaced every two days. In some experiments, 50 ng/ml FGF10, 50 ng/ml HGF, 20 ng/ml NOG, 10 nM TSA, or 100 nM SAHA was added to the TS medium (see [Table S2](#)). When cells reached 60%–80% confluence, they were dissociated with TrypLE for 10–15 min at 37°C and passaged to a new Col IV-coated 6-well plate at a 1:2–1:4 split ratio. The CT cells initially grew slowly but gave rise to highly proliferative TS^{CT} cells within several passages. Thereafter, TS^{CT} cells were routinely passaged every two days at a 1:4 split ratio. Unless otherwise indicated, TS^{CT} cells at passages 10–20 were used for analysis.

Frozen-thawed human blastocysts (5–6 days post-fertilization) were treated with Tyrode's solution to remove the zona pellucida. Each blastocyst was placed in Col IV-coated 4-well plate and cultured in 400 μ L of TS medium. After 4–5 days of culture, the blastocyst outgrowth was dissociated with TrypLE for 5–10 min at 37°C and passaged to a new Col IV-coated 4-well plate. TS^{blast} cells

emerged within several passages and were routinely passaged every two days at a 1:4 split ratio. Unless otherwise indicated, TS^{blast} cells at passages 10–20 were used for analysis.

Stromal cells were cultured on gelatin-coated dishes with DMEM supplemented with 10% FBS, 1 mM sodium pyruvate, 2 mM L-glutamine, and 1% Penicillin-Streptomycin, and used for immunofluorescence analysis within seven passages.

For cryopreservation, TS^{CT}, TS^{blast}, and stromal cells were suspended in Cell Banker 1 and stored in a deep freezer at -80°C or liquid nitrogen.

Differentiation of TS^{CT} and TS^{blast} cells

TS^{CT} and TS^{blast} cells were grown to $\sim 80\%$ confluence in the TS medium and dissociated with TrypLE for 10–15 min at 37°C . For the induction of EVT-TS^{CT} and EVT-TS^{blast} cells, TS^{CT} and TS^{blast} cells were seeded in a 6-well plate pre-coated with $1\ \mu\text{g/ml}$ Col IV at a density of 0.75×10^5 cells per well and cultured in 2 mL of EVT medium [DMEM/F12 supplemented with 0.1 mM 2-mercaptoethanol, 0.5% Penicillin-Streptomycin, 0.3% BSA, 1% ITS-X supplement, 100 ng/ml NRG1, 7.5 μM A83-01, 2.5 μM Y27632, and 4% KnockOut Serum Replacement]. Matrigel was added to a final concentration of 2% shortly after suspending the cells in the medium. At day 3, the medium was replaced with the EVT medium without NRG1, and Matrigel was added to a final concentration of 0.5%. After the cells reached $\sim 80\%$ confluence at day 6, they were dissociated with TrypLE for 15–20 min at 37°C and passaged to a new Col IV-coated 6-well plate at a 1:2 split ratio. The cells were suspended in the EVT medium without NRG1 and KSR, Matrigel was added to a final concentration of 0.5%, and cultured for two additional days.

For the induction of ST(2D)-TS^{CT} and ST(2D)-TS^{blast} cells, TS^{CT} and TS^{blast} cells were seeded in a 6-well plate pre-coated with 2.5 $\mu\text{g/ml}$ Col IV at a density of 1×10^5 cells per well, and cultured in 2 mL of ST(2D) medium [DMEM/F12 supplemented with 0.1 mM 2-mercaptoethanol, 0.5% Penicillin-Streptomycin, 0.3% BSA, 1% ITS-X supplement, 2.5 μM Y27632, 2 μM forskolin, and 4% KSR]. The medium was replaced at day 3, and the cells were analyzed at day 6.

For the induction of ST(3D)-TS^{CT} and ST(3D)-TS^{blast} cells, 2.5×10^5 TS^{CT} and TS^{blast} cells were seeded in 6 cm Petri dishes and cultured in 3 mL of ST(3D) medium [DMEM/F12 supplemented with 0.1 mM 2-mercaptoethanol, 0.5% Penicillin-Streptomycin, 0.3% BSA, 1% ITS-X supplement, 2.5 μM Y27632, 50 ng/ml EGF, 2 μM forskolin, and 4% KSR]. An equal amount of fresh ST(3D) medium was added at day 3. The cells were passed through a 40 μm mesh filter to remove dead cells and debris at day 6. We collected and analyzed ST(3D)-TS^{CT} and ST(3D)-TS^{blast} cells remaining on the 40 μm mesh filter.

RNA-seq

Total RNA was extracted with the RNeasy mini Kit and RNase-free DNase (QIAGEN, CA, USA) and used for library construction employing the TruSeq Stranded mRNA LT Sample Prep Kit (Illumina, San Diego, CA) according to the manufacturer's protocol. RNA integrity was assessed using TapeStation 2200 (Agilent Technologies, Santa Clara, CA). All primary samples had an RNA integrity number equivalent (RIN^e) value of > 7 , and all cultured samples had an RIN^e value of > 9 . The libraries were sequenced on the Illumina HiSeq 2500 platform (Illumina) with 101-bp paired-end reads. The reads were aligned to the reference genome (UCSC hg19) using TopHat (Trapnell et al., 2012) with the Refseq gene annotation. For female samples, the Y chromosome was excluded from the reference genome. Expression levels (FPKM) of Refseq genes were calculated using Cufflinks (Trapnell et al., 2012). Differentially expressed genes were identified using DESeq2 (Love et al., 2014). X-linked genes in the pseudoautosomal regions and Y-linked genes were excluded from the analysis.

MiRNA-seq

Total RNA was prepared from freshly frozen $\sim 1 \times 10^6$ cells using AllPrep DNA/RNA/miRNA Universal Kit (QIAGEN). Small RNA libraries were prepared using the NEBNext Small RNA Library Prep Set for Illumina (NEB, Ipswich, MA) according to the manufacturer's protocol. The synthesized cDNAs were used as templates for PCR amplification (10–12 cycles). Amplified DNA fractions corresponding to the size range of the adaptor-ligated small RNAs were isolated from the gel. The product size was measured using a High Sensitivity DNA kit (Agilent Technologies). The yield of the small RNA library was measured by quantitative RT-PCR using a KAPA Library Quantification Kit (KAPA Biosystems, Woburn, MA), and the library concentration was adjusted to 8 pM. A PhiX Control Kit (Illumina) was used as a spike-in control for sequencing. Single-end runs were performed on Illumina HiSeq 1500 platform. Raw sequence reads were first trimmed to remove the adaptor sequences. Then, the trimmed reads (20–24 nucleotides) were mapped to human miRNAs (hg19), which were retrieved from miRBase v19 (Kozomara and Griffiths-Jones, 2014), using BLASTN program. The reads that showed 100% nucleotide identity to miRNAs were used for the analysis.

WGBS

WGBS was performed using the post-bisulfite adaptor-tagging (PBAT) method (Miura et al., 2012). Briefly, genomic DNA was purified with phenol/chloroform extraction and ethanol precipitation. Genomic DNA spiked with 0.5% (w/w) unmethylated lambda phage DNA (Promega, Madison, WI) was used for library preparation according to the PBAT protocol. Concentrations of the PBAT products were quantified using the KAPA Library Quantification Kit for Illumina platforms (Kapa Biosystems). PBAT libraries were sequenced on the Illumina HiSeq 1500 (Illumina) equipped with HCS v2.0.5 and RTA v1.17.20 with 101-bp single-end reads. The reads were aligned to the reference genome using Bismark (Krueger and Andrews, 2011). The methylation level of each cytosine was calculated using the Bismark methylation extractor. For each CpG site, reads from both strands were combined to calculate the methylation level. Methylation levels of CpGs covered with ≥ 5 reads were analyzed.

Targeted bisulfite sequencing (BS)

Targeted BS was performed as described previously (Hamada et al., 2016). Briefly, genomic DNA was sheared and custom sequencing adapters were ligated using the NEBNext Ultra Ligation Module (NEB). Target regions were enriched using the SureSelect Custom Target Enrichment kit (Agilent Technologies, Santa Clara, CA). The enriched fragments were treated with sodium bisulfite using the EZ DNA Methylation-Lightning Kit (Zymo Research, Orange, CA) and amplified for 10 cycles using the KAPA HiFi HotStart Uracil+ ReadyMix PCR Kit (KAPA Biosystems). The libraries were sequenced on the Illumina HiSeq 2500 platform (Illumina) with 101-bp paired-end reads. The first 2 bases and the last 1 were trimmed from the forward reads and the first 5 bases and the last 1 were trimmed from the reverse reads. The trimmed reads were aligned to the reference genome with Bismark. SNPs distinguishing parental alleles were identified using TS^{CT} cell lines and the maternal blood cells as described previously (Hamada et al., 2016). Paired-end reads containing SNPs were extracted from the uniquely mapped reads obtained by the targeted BS analyses. The reads were classified into maternal reads and paternal reads according to the SNP alleles. The methylation level of each cytosine was calculated using the maternal and paternal reads separately. For each CpG site, reads from both strands were combined to calculate the methylation level. For allelic methylation analyses, we used only methylation levels of CpGs that were covered with ≥ 5 reads for both maternal and paternal alleles and were not overlapping SNPs. Only gDMRs containing ≥ 5 informative CpGs were analyzed. Maternal and paternal methylation are defined as [Maternal methylation level] - [Paternal methylation level] $\geq 30\%$ and $\leq -30\%$, respectively.

Allelic expression analysis

Allelic expression analysis was performed as described previously (Hamada et al., 2016). To identify SNPs distinguishing parental alleles, exome-sequencing was performed using TS^{CT} cells and the mother's peripheral blood cells. Exome-sequencing libraries were constructed using the SureSelect Human All Exon V5+UTRs Kit (Agilent Technologies) according to the manufacturer's instructions. Libraries were sequenced on the Illumina HiSeq 2500 platform (Illumina) with 101-bp paired-end reads. The reads were aligned to the reference genome and SNPs were called. RNA-seq was performed as described above, and uniquely mapped reads were kept. We analyzed only SNPs covered with ≥ 20 reads and the numbers of paternal and maternal reads were counted for each gene.

Combined bisulfite restriction analysis (COBRA)

Genomic DNA was purified with phenol/chloroform extraction and ethanol precipitation and treated with sodium bisulfite using the EZ DNA Methylation-Lightning Kit and amplified with TaKaRa EpiTaq HS (Takara Bio, Shiga, Japan). The PCR products were digested with HhaI and analyzed with TapeStation 2200.

Immunostaining

Cells were fixed with 4% paraformaldehyde (PFA) for 10 min, permeabilized with 0.3% Triton X-100 for 5 min, and blocked with 2% FBS/PBS for one hour at room temperature. The cells were then incubated with the primary antibodies overnight at 4°C. The following primary antibodies were used: PE-conjugated anti-ITGA6 (1:100), PE-conjugated anti-HLA-G (1:100), PE-conjugated anti-SDC1 (1:100), anti-TP63 (1:100), anti-GATA3 (1:100), anti-TEAD4 (1:200), anti-CDH1 (1:100), anti-hCG (1:10), and anti-VIM (1:100). Alexa Fluor 488- or Alexa Fluor 555-conjugated secondary antibodies were used as secondary antibodies. Nuclei were stained with Hoechst 33258, and the images were taken with a fluorescence microscope (BZ-X710, Keyence, Osaka, Japan) or a laser scanning confocal microscope (LSM780, Carl Zeiss, Germany).

Frozen sections were permeabilized with 0.3% Triton X-100 for 5 min, blocked in 2% goat serum in TBST for one hour, and incubated with primary antibodies at 4°C overnight. The sections were then incubated with fluorescent-labeled secondary antibodies for one hour. Paraffin sections were boiled in citric acid buffer (pH 6.0), blocked in 2% goat serum in TBST for one hour, and incubated with primary antibodies at 4°C overnight. The sections were then incubated with HRP-conjugated secondary antibodies for one hour. The HRP-conjugated antibodies were detected with diaminobenzidine (DAB). The following primary antibodies were used: anti-KRT7 (1:50), anti-ITGA6 (1:50), PE-conjugated anti-SDC1 (1:50), and anti-HLA-G (1:30). The images were obtained with BZ-X710.

Flow cytometry

Cells were dissociated with TrypLE, passed through a 70 μm mesh filter, and suspended in 2% FBS/PBS. For flow cytometric analysis of KRT7, cells were fixed with 4% PFA for 10 min at room temperature, and permeabilized with 0.1% Triton X-100 for 10 min. The cells were then incubated with an anti-KRT7 antibody (1:50) for an hour and stained with Alexa Fluor 488-conjugated anti-rabbit IgG for 45 min. Normal rabbit IgG was used as isotype control. For flow cytometric analysis of HLA-ABC and HLA-G, unfixed cells were incubated with an FITC-conjugated anti-HLA-ABC antibody (1:50) or a PE-conjugated anti-HLA-G antibody (1:50) for 15 min at room temperature. FITC-conjugated mouse IgG2a or PE-conjugated mouse IgG1 was used as isotype control. Flow cytometry was carried out using a FACSAria II, and the data were analyzed using FlowJo software.

Measurement of hCG

TS^{CT} and TS^{blast} cells were seeded at a density of 0.5×10^5 cells/ml and differentiated into ST-like cells as described above. The medium was replaced at day 4, and the supernatants were collected at day 6 and stored at -80°C . As controls, TS^{CT} and TS^{blast} cells were seeded at a density of 0.5×10^5 cells/ml and cultured in the TS medium. At day 2, the supernatants were collected and stored at -80°C . The amount of secreted hCG was measured using an hCG ELISA kit. Serum hCG levels were also measured with the same kit.

Quantitative real-time PCR analysis

Total RNA was prepared using an RNeasy mini Kit and RNase-free DNase (QIAGEN). First-strand cDNA was synthesized from total RNA using PrimeScript II (Takara Bio), and real-time PCR reaction was done with the StepOnePlus Real-Time PCR System (Applied Biosystems, Foster City, CA) and SYBR Premix Ex TaqII (Takara Bio). The amount of target mRNA was determined using the $\Delta\Delta C_t$ method with *GAPDH* as the internal control. The *CSH1/2* primers amplify both *CSH1* and *CSH2*.

Chromosome analysis

Genomic DNA was purified with phenol/chloroform extraction and ethanol precipitation, and whole-genome sequencing (WGS) libraries were constructed using the TruSeq Nano DNA LT Sample Prep Kit (Illumina) according to the manufacturer's instructions. Libraries were sequenced on the Illumina HiSeq 2500 platform (Illumina) with 101-bp paired-end reads. We obtained 10–15 million reads for each sample, and the reads were aligned to the reference genome using Bowtie2 with default parameters. Each chromosome was divided into 1 Mb-windows and reads per million mapped reads (RPM) were calculated for each window. The RPM values were normalized to those of karyotypically normal CT cells and smoothed over 10 Mb. We only considered windows with > 50 RPM in the control CT cells. The thresholds for copy number gain and loss were set at 2.3 and 1.7 copies, respectively. For the X chromosome in male cells, the thresholds were set at 1.3 and 0.7.

Engraftment of TS cells into NOD-SCID mice

TS cells were grown to ~80% confluence in the TS medium and dissociated with TrypLE. 10^7 TS cells were resuspended in 200 μ L of a 1:2 mixture of Matrigel and DMEM/F12 containing 0.3% BSA and 1% ITS-X supplement, and subcutaneously injected into 6- to 8-week-old male NOD-SCID mice. Lesions and serum were collected seven days after injection. The lesions were fixed with 4% PFA overnight at 4°C followed by cryoprotection in 30% sucrose or embedding in paraffin. Cryopreserved and paraffin-embedded tissues were sectioned at 5 μ m. Sections were stained with hematoxylin-eosin (H&E) or processed for immunostaining as described above.

Annotations of genomic regions and differentially expressed genes

Annotations of Refseq genes were downloaded from the UCSC Genome Browser. Promoters were defined as regions 1 kb upstream and downstream of transcription start sites. The gene bodies were defined as transcribed regions of Refseq transcripts except for promoters. Promoters of Refseq genes shorter than 300 bp (encoding microRNAs or small nucleolar RNAs in most cases) were excluded from our analyses. gDMRs were defined as previously reported (Hamada et al., 2016). Functional annotation of differentially expressed genes was performed using the ConsensusPathDB human pathway database (Herwig et al., 2016). GSEA was performed using GSEA version 3.0.

Graphical presentation

Methylation levels of CpGs were visualized using Integrative Genomics Viewer (IGV) software (Robinson et al., 2011). Heatmaps and scatterplots were generated using the heatmap.2 function of the gplots package and the heatscatter function of the LSD package in R, respectively. Violin plots were generated using the vioplot package.

External data

The RNA-seq data for CT (Japanese Genotype-phenotype Archive (JGA) accession numbers: JGAX00000007522, JGAX00000007532, and JGAX00000007538) and the WGBS data for CT (JGA accession number: JGAX00000007488) and cord blood cells (DNA Data Bank of Japan (DDBJ) accession numbers: DRX036834–8) were from our previous studies (Hamada et al., 2016; Okae et al., 2014). We also included available WGBS data for human ES cells (Gene Expression Omnibus (GEO) accession number: GSM706059) (Lister et al., 2011) and miRNA-seq data for human ES cells (GEO accession number: GSM438362) and IMR90 cells (GEO accession number: GSM438364).

QUANTIFICATION AND STATISTICAL ANALYSES

The sample size for each experiment is given in the figure legend. The “n” represents the number of cell lines or placental samples in Figures 4C–4E and experimental replicates in Figures 1B, 2E and 2I, and 3K and Figures S1F and S2G. We isolated 10 clonal lines from a TS^{CT} line (Figures 2J and 2K) and 8 clonal lines from a TS^{blast} line (Figures 3L and 3M). Statistical analysis was performed using Statcel software (OMS, Saitama, Japan) or R (version 3.3.1), and a p value < 0.05 was considered statistically significant.

DATA AND SOFTWARE AVAILABILITY

All sequencing data reported in this paper are deposited in the JGA under the accession numbers JGA: JGA00000000074, JGA: JGA00000000117, and JGA: JGA00000000122.